Origin and evolution of the slab fluids since subduction inception in the Izu-Bonin-Mariana: A comparison with the southeast Mariana fore-arc rift

Julia Ribeiro[1], Christopher MacLeod[2], Johan Lissenberg[2], Jeff Ryan[3], Colin Macpherson[4]

[1]State Key Laboratory of Isotope Geochemistry, Guangzhou Institute of Geochemistry, Chinese Academy of Sciences, Guangzhou 510640, China.

[2] Department of Earth and Environmental Sciences, Cardiff University, Cardiff, Wales, CF10 3AT, UK.

[3] University of South Florida, School of Geosciences, Tempa, FL, USA.

[4] Department of Earth Science, Durham University, Durham, UK.

Abstract

Subduction zones have played a central role in exchanging volatiles (H_2O, CO_2, S, halogens) between the different Earth's reservoirs throughout its history. Fluids that are released as the subducted plates dehydrate are major agents that transfer these volatiles inside the Earth; but the origins and the compositional evolution of the slab fluids as plates begin to sink are yet to be understood. To explore processes that take place during subduction infancy, here we examine the compositions of proto-arc magmas from the Izu-Bonin-Mariana (IBM) convergent margin that formed during subduction inception; and we compare these to a modern example of near-trench spreading in the southeast Mariana fore-arc rift (SEMFR). There is a temporal and spatial evolution in the slab fluid composition that is accompanied with a change in the fluid reservoirs, as subduction progresses. During the early stages of the subduction zone, dehydration of the serpentinized subducting mantle likely triggered dehydration and melting of the altered oceanic crust in the amphibolite facies to produce boninites. As the subduction zone matured, the volcanic arc front was displaced away from the trench. The arc magmas captured deeper slab fluids released from the subducted oceanic crust, the sediments and the

underlying serpentinized mantle. Dehydration and melting of the subducted sediment became more prevalent with time and increasing slab depth (≥ 100 km) to produce arc magmas. This compositional evolution was associated with a deepening of magma generation, which is likely accompanied with the progressive serpentinization of fore-arc mantle. Hence, fore-arc mantle serpentinization might have facilitated arc maturation and subduction stabilization throughout the IBM history.

1- Introduction

Subduction zones have efficiently cycled volatiles (H_2O, S, Cl, F, CO_2) between the Earth's interior and the hydrosphere - atmosphere over geological time. The varying fluxes of volatiles released at subduction zones have regulated explosive volcanism, which, in return, has modulated and Earth's climate and habitability for millions of years.

During subduction, the subducted sediments are believed to dehydrate first, at about ~50 to 100 km depths, releasing water-rich slab fluids enriched in volatiles (CO_2, H_2O, S, Cl) and in fluid-mobile elements (Cs, Rb, Ba, Pb, U). These water-rich slab fluids serpentinize the relatively cool (~ 600^{o}C) fore-arc mantle wedge at shallow slab depth (< 100 km depth) (Hyndman and Peacock, 2003; Rüpke et al., 2004; Savov et al., 2007). Dehydration of subducted altered oceanic crust and serpentinized mantle occur at greater depths, of ~100 – 200 km depths, to trigger magmatism beneath the volcanic arc front and the back-arc basin (Elliott et al., 1997; Grove et al., 2006; Pearce et al., 2005; Rüpke et al., 2004). As subduction proceeds, the slab-derived fluids become less water-rich; and they progressively transition into solute-rich slab fluids derived from sediment melting (or sediment melts) with increasing slab depth (≥ 100 km) (Johnson and Plank, 1999; Kessel et al., 2005; Manning, 2004). Volatile liberation from the incoming plate is discontinuous to sub-arc depth (Muñoz-

Montecinos et al., 2021), and the slab's capacity to carry water and other volatiles diminishes with increasing depth (Rüpke et al., 2004; Schmidt and Poli, 1998). Although our understanding of the formation and role of slab fluids has improved significantly over the past decades, questions still remain regarding their origins and temporal-spatial compositional evolution as subduction begins and the slab sinks progressively deeper. We can wonder if this long-standing model also holds during the early development of a subduction zone and throughout its lifespan. Does the composition of the slab fluids evolve over time? Are the fluids released from the same part of the subducting slab during subduction maturation?

To address these questions, we compiled a dataset from the Izu-Bonin-Mariana (IBM) proto-arc crust (i.e., fore-arc basalts and boninites), the infant arc, and the mature volcanic arc to examine the temporal variations in the compositions and in the sources of slab fluids since subduction inception. We further compare the IBM proto-arc magmas to those from the Southeast Mariana fore-arc rift (SEMFR), which developed by near-trench spreading long after subduction initiated, to place additional constraints onto the subduction processes that occur relatively close (within ~ 90 km) to the trench. We find that the slab fluid compositions evolved over the lifetime of IBM. This compositional evolution reveals a change in the sources of the slab fluids, which is associated with the progressive migration of the volcanic arc front and a deepening of magma generation.

2- Geological background

2.1- Temporal evolution of the IBM convergent margin

The Izu-Bonin-Mariana fore-arc crust has long been regarded as a typical example of proto-arc crust that developed during subduction inception (Fig. 1A) (Ishizuka et al., 2006; Reagan et al., 2010; Stern and Bloomer, 1992). The IBM subduction zone is associated with

78 the sinking of the Pacific plate underneath the Philippine Sea plate, which initiated about 52
79 Myr ago (Fig. 2). Rapid sinking of the nascent slab enabled spreading of the proto-arc
80 oceanic lithosphere in front of the trench (called hereafter near-trench spreading) (Ishizuka et
81 al., 2006; Reagan et al., 2010; Stern and Bloomer, 1992). Hence, the asthenospheric mantle
82 flowed into the mantle wedge (i.e., the future fore-arc) and melted right above the descending
83 plate, producing new oceanic crust in front of the trench (Fig. 1A) (Ishizuka et al., 2006;
84 Maunder et al., 2020; Reagan et al., 2010). Several types of magmas were produced over the
85 IBM lifetime, as the subduction zone evolved; and these include:
86
87 • *Tholeiitic proto-arc basalts* (also named fore-arc basalts or FABs in the literature, after
88 Reagan et al. (2010)) which represent the first magmas emplaced as the slab began
89 sinking. These formed by decompression melting of the proto-arc asthenosphere with
90 limited infiltration of slab fluids from 52 to 48 Myr (Maunder et al., 2020; Pearce et
91 al., 1984; Reagan et al., 2010; Stern and Bloomer, 1992). Proto-arc lithosphere
92 accreted by spreading in front of the trench (i.e., near-trench spreading) during
93 subduction inception (Coulthard et al., 2021; Ishizuka et al., 2006; Ishizuka et al.,
94 2011a; Reagan et al., 2017).
95
96 • *Low-silica boninites (LSB)* which formed shortly after the FABs by near-trench
97 spreading from 51 to 48 Myr (Coulthard et al., 2021; Ishizuka et al., 2006; Reagan et
98 al., 2010; Shervais et al., 2019). As the subducted slab began to dehydrate and melt,
99 the resulting slab-derived fluids infiltrated the residual, depleted proto-arc
100 asthenosphere to produce the LSB (Ishizuka et al., 2006; Pearce and Reagan, 2019;
101 Reagan et al., 2017).
102

- Seafloor spreading rapidly transitioned into fluid-assisted mantle melting due to the increasing fluxing of the depleted asthenosphere by the slab fluids, which produced *high-silica boninites (HSB)* from 50 to 45 Myr (Coulthard et al., 2021; Li et al., 2019; Pearce and Reagan, 2019; Reagan et al., 2010; Reagan et al., 2017; Shervais et al., 2021; Stern and Bloomer, 1992) (Fig. 1A). The progressive compositional evolution from the FABs to the high-Si boninites further implies that near-trench spreading continuously transitioned from decompression mantle melting to fluid-assisted mantle melting within 5-10 Myr following subduction inception (Coulthard et al., 2021; Ishizuka et al., 2006; Ishizuka et al., 2011a; Reagan et al., 2010; Shervais et al., 2021; Stern and Bloomer, 1992). HSB developped as small volcanic cones only a few kilometers from the trench. Some of these volcanoes have been preserved in the IBM fore-arc (Bonin Island, now called Chichijima; Fig. 2) (Reagan et al., 2010; Reagan et al., 2017). Boninites represent the onset of arc magmatism, as they are the first melts that formed by fluid-assisted mantle melting (Ishizuka et al., 2011a; Pearce and Reagan, 2019; Reagan et al., 2010).

- *Infant arc magmas* appeared shortly after the eruption of the high-Si boninites, i.e. from 45 to 41 Myr (Ishizuka et al., 2020; Ishizuka et al., 2011b; Reagan et al., 2017). These represent the youngest arc volcanoes, which rapidly form within 10 Myr of subduction inception (Ishizuka et al., 2006; Ishizuka et al., 2011b; Kanayama et al., 2012). Arc infancy is a transient and short-lived stage (that lasted ~ 5 Myr) during which small submarine and subaerial volcanic cones rapidly developed and migrated away from the trench, without consolidating magma generation (Ishizuka et al., 2011a; Ishizuka et al., 2020; Ribeiro et al., 2019). Some of these early arc volcanoes are

preserved in the Bonin Islands (Fig. 2) (Ishizuka et al., 2006; Kanayama et al., 2012, 2014).

- *The mature volcanic arc* began to develop from ~ 40 - 42 Myr and remains active (Baker et al., 2008; Ishizuka et al., 2011b; Stern et al., 2013a; Tamura et al., 2014; Tamura et al., 2011). The volcanic arc front has stabilized at its current location at ~ 150 km from the trench the past 40 Myr (Ishizuka et al., 2011b; Straub et al., 2010; Straub et al., 2015), and it lies ~ 100 - 150 km depth above the slab surface (Stern et al., 2003). Magma generation has consolidated over time through the formation of dykes and sills. This continuous supply of melts underneath the mature arc promoted crustal thickening and magma differentiation.

As the IBM subduction zone matured and stabilized into a long-lived convergent margin, progressive serpentinization of the fore-arc mantle was accompanied by the retreat of the infant volcanic arc front until stabilization. Hence, the conditions for a mature subduction zone were rapidly established in IBM (≤ 10 Myr) (Ishizuka et al., 2006; Ishizuka et al., 2020; Ishizuka et al., 2011b; Ribeiro et al., 2019; Straub et al., 2010; Straub et al., 2015).

2.2- The southern Mariana fore-arc rift (SEMFR)

The southern Mariana intra-oceanic arc represents the southern end of the Izu-Bonin-Mariana (IBM) convergent margin (Fig. 2). To the south, Eocene proto-arc crust, that formed during subduction infancy (Reagan et al., 2010), has undergone recent extension (< 5 Myr) to accommodate opening of the Mariana Trough (Martinez et al., 2000; Martinez et al., 2018). As a result, the southeast Mariana fore-arc rifts (SEMFR) opened in front of the trench due to large-scale and disorganized lithospheric stretching above the shallow part of the subducting

Pacific plate (< 100 km depth to the slab), long after subduction had initiated (Fig. 1B). Slab dehydration probably enhanced magmatic activity, resulting in a 6-km-thick and homogeneous basaltic crust in the Mariana fore-arc (Martinez et al., 2018; Ribeiro et al., 2013b). To the northwest, the SEMFR progressively transitions into the Fina-Nagu volcanic chain (FNVC), which represents a juvenile arc that initiated less than 5 Myr ago (Brounce et al., 2016; Ribeiro et al., 2019; Stern et al., 2013b). Near-trench spreading aborted within ~2 Myr (Martinez et al., 2018; Ribeiro et al., 2013a); and the inflated spreading ridges collapsed as soon as magmatic activity ceased, forming the actual fore-arc rifts.

The SEMFR is now floored with recently erupted basaltic pillow lavas and lava flows within 80-90 km from the trench (Martinez et al., 2018; Ribeiro et al., 2013a). The basalts are underlain by a gabbroic lower crust and by a mixture of harzburgitic and refertilized lherzolitic mantle (Michibayashi et al., 2009; Ohara and Ishii, 1998; Ribeiro et al., 2013a). Even though near-trench spreading in the southern Marianas occurred long after subduction initiated, the formation of new seafloor above a shallow dehydrating slab may be analogous to the processes that occur during subduction inception. Hence, examining the SEMFR magmas can provide critical insights into the shallow and near-trench subduction processes, which are rarely captured in modern subduction zones.

3- **Data compilation and filtering**

To place additional constraints upon the processes that developed during subduction infancy, we compiled a dataset (n = 1132) that includes bulk rock analyses and *in-situ* micro-analyses of glasses from the SE Mariana fore-arc rift (SEMFR), the Izu-Bonin-Mariana proto-arc crust, and the Mariana arc and back-arc. Fresh glass shards and olivine-hosted melt inclusions were selected whenever possible, as they may have retained their primitive melt

177 compositions more faithfully than their host rock. Additionally, glass shards and olivine-
178 hosted melt inclusions have experienced the least degassing, and so may provide additional
179 constraints onto the volatile contents of water-rich slab fluids.
180
181 Because magmas degas upon ascent or during eruption, so fresh glass shards and
182 olivine-hosted melt inclusions were filtered for minimally degassed volatile contents (CO_2 >50
183 ppm and S >500 ppm), as in Kelley et al. (2006). Samples were then screened for basaltic (SiO_2
184 ≤ 56 wt%) and boninitic compositions (i.e., as reported in the literature) with a total sum of
185 oxides equal to 100 ± 2 wt% to ensure freshness and filtering for highly fractionated magma
186 compositions, as some fractionating mineral phases (amphibole, ilmenite, biotite, …) could
187 modify trace element ratios (Schiano, 2003). Boninites are not excluded of our database for
188 high silica content, as neither low- nor high-silica boninites crystallize the mineral phases
189 which could modify their incompatible element ratios (i.e., olivine, spinel, orthopyroxene)
190 (Pearce et al., 2005). This filtering (n = 521) allows us to minimize the effects of volatile
191 degassing, alteration, crustal assimilation and contamination to ensure that the composition of
192 the magmas is most representative of their sources. Our filtered dataset includes 20 olivine-
193 hosted melt inclusions and 13 basaltic glass shards from the SEMFR, 203 olivine-hosted melt
194 inclusions, 11 basaltic glass shards and 29 bulk rocks from the Mariana arc, 46 bulk rocks and
195 47 basaltic glass shards from the Mariana Trough, 72 glass shards from the IBM proto-arc
196 crust, and 75 bulk rocks from the infant arc.
197 The water content of the glasses was also compared to incompatible elements, such as
198 Rb, that are mobilized with the aqueous slab fluids but remain unaffected by volatile degassing.
199 Correlations between water, Rb, MgO and SiO_2 indicates that the filtered dataset (i) glasses
200 have probably lost little water by degassing (Fig. S1-S4); and (ii) the melt inclusions did not
201 experience diffusive re-equilibration with the host olivine (Gaetani et al., 2012) . This filtered

dataset was used to examine the composition of slab fluids. However, we also used the complete dataset to examine major element composition of the magmas as well as their Pb-Sr isotopic ratios, which are rarely measured on fresh glass shards.

Despite their freshness, glasses can still be prone to secondary alteration processes after being emplaced onto the seafloor. They can also have captured hydrothermal brines within the magma chamber or upon ascent (Kent et al., 1999). Elements of interest (Ba, Rb, Th, H_2O, …) were plotted against elements that are believed to remain immobile during alteration processes (see supplementary Fig. S1-S4). Fractionation trends were mostly preserved, indicating that magmas were little affected by alteration (Fig. S1-S4). Hence, their composition can be used to reliably track the composition of the slab fluids that infiltrated their mantle source. The complete and the filtered datasets are reported in Table S1. Details and references can be found in the supplementary material.

4- Magma composition

4.1- From the IBM proto-arc to the mature arc magmas

The IBM FABs are characterized by low K_2O (< 1 wt%) and low water contents (H_2O = 0.75 ± 0.58 (1σ) wt%) (Fig. 3A). They are however slightly enriched in water compared with mid-ocean ridge basalts (H_2O < 0.2 wt%) (Saal et al., 2002). The low-silica (LSB) and the high-silica boninites (HSB) possess higher K_2O content (> 0.2 wt%) and higher water content (H_2O = 3.68 ± 1.21 (1σ) wt%) than the FABs (Fig. 3A). They are characterized by low TiO_2 content (< 0.4 wt%) (Fig. 3B) compared with the Mariana arc magmas, which indicates melting of a strongly depleted, residual mantle source (Pearce and Reagan, 2019; Reagan et al., 2017). In the MgO vs. SiO_2 diagram of Pearce and Reagan (2019), the FABs, the LSB and the HSB plot along distinct liquid lines of descent, demonstrating that they did not form

during the same melting event. From the FABs to the HSB, there is an increase in the SiO_2 and K_2O contents of the magmas over time (stages 1 to 3 in Fig. 3A).

The infant arc magmas are low-K to medium-K basalts to dacites (Fig. 3A). As the arc reaches maturity, the magmas become more enriched in K_2O, so that the mature arc magmas are medium-K basalts to dacites. The infant arc magmas thus contrast with the more mature Mariana arc by having lower K_2O content (Fig. 3A). This increase in the K_2O content of the magmas during subduction maturation reveals the progressive migration and deepening of the magma generation with time. Indeed, K-rich phases within the subducted slab, such as lawsonite and phengite, tend to breakdown at sub-arc depth, so that the near-trench magmas that overly a shallower part of the slab (≤ 90 km depth), capture K-poor, water-rich slab fluids. By contrast, the infiltration of K-rich, water-rich aqueous slab fluids into the sub-arc mantle enriches the arc magmas in K (Hatherton and Dickinson, 1969; Kimura and Stern, 2008; Pearce and Robinson, 2010; Plank and Langmuir, 1993; Schmidt and Poli, 1998) (Fig. 4-5). The low K_2O content of the early IBM magmas is thus consistent with their formation within ~ 90 - 100 km from the trench and above a shallow, nascent subducted slab. The mature arc magmas formed instead at ~ 150 – 200 km from the trench, and they overlie a deeper portion of the slab (~ 100 km depth).

4.2- The SEMFR magmas

The SEMFR magmas are low-K basalts (SiO_2 < 59 wt%, K_2O ≤ 1 wt%) (Fig. 3A), and contain 1.84 ± 0.39 (1σ) wt% H_2O on average. In terms of SiO_2, K_2O, MgO and TiO_2 contents, the SEMFR basalts are similar to FABs. Their higher TiO_2 content (> 0.4 wt%) compared with the boninites (Fig. 3B), reveal that they formed by melting of a relatively undepleted mantle source, as also shown by their Nb/Yb ~ 1 (Fig. 4).

The SEMFR basalts host some olivine mantle xenocrysts (Fo_{90-92}), which can enclose fresh melt inclusions. The melt inclusions occur as isolated pieces of melt that are fully entrapped by their olivine host. The melt inclusions were perhaps entrapped at ~ 22.0 ± 6.6 km depth during olivine growth (Ribeiro et al., 2015). The SEMFR olivine-hosted melt inclusions are primitive basalts (MgO > 8 wt%, SiO_2 < 54 wt%) that possess low K_2O (< 1 wt%) and low TiO_2 (< 0.5 wt%) contents (Fig. 3). In the classification diagram of Pearce and Reagan (2019), the olivine-hosted melt inclusions overlap the compositional field for the LSB (Fig. 3). This suggests melting of a more depleted mantle source than that of their host lavas, and is consistent with their lower Nb/Yb ratios (~ 0.1) (Fig. 4). Ribeiro et al. (2015) suggested that the SEMFR olivine-hosted melt inclusions trapped melts that formed by adiabatic decompression mantle of the refractory fore-arc asthenosphere, that was infiltrated by the water-rich slab fluids released during shallow slab dehydration. They proposed that the recent stretching of the Eocene fore-arc lithosphere in the southern Marianas (~ 5 Myr ago) enabled the fore-arc asthenosphere to flow in and melt under highly hydrous conditions within 90 km from the trench. Near-trench spreading allowed the SEMFR magmas to erupt in Pliocene time, while they captured mantle olivine upon ascent.

5- Compositional evolution of the slab fluids since subduction inception

Slab dehydration and slab melting can be inferred using chemical proxies (e.g., Rb/Th, Cs/Th, H_2O/Ce, Th/Nb, La/Sm, Hf/Sm and Zr/Sm), which represent a record of the water-rich and solute-rich slab fluids that participate in mantle melting (Elliott et al., 1997; Johnson and Plank, 1999; Manning, 2004; Pearce et al., 2005). Ratios of a fluid-mobile element (Ba, Cs, Rb, H_2O, Th, La) over an incompatible element that is not mobilized with the fluids (Nb, Yb, Sm, Ce), but migrate similarly during mantle melting, has the advantage to minimize for fractionation and melting processes. Hence, elemental ratios can preserve a reliable signature

of the slab fluids (Kogiso et al., 1997; McCulloch and Gamble, 1991). Because Ba, Rb and Cs are mobilised by both with the water-rich fluids and the sediment melts, Rb/Th, Cs/Th and Ba/Th ratios will track the water-rich slab fluids (Fig. 4–5), as Th is mainly mobilized during sediment melting (Johnson and Plank, 1999; Pearce et al., 2005). Similarly, H_2O/Ce has been used as a marker of water-rich slab fluids, as Ce remains relatively immobile with the water-rich slab fluid (Dixon et al., 2017; Dixon et al., 2002; Ruscitto et al., 2012). The Ba/Nb, Rb/Nb and Cs/Nb ratios track instead the total subduction signal (i.e., water-rich fluid and solute-rich fluid); while Th/Nb ratios track the solute-rich fluids released during sediment melting (Elliott et al., 1997; Pearce et al., 2005).

Hf/Sm and Zr/Sm ratios have been proposed to track melting of the oceanic crust in the amphibolite facies (Foley et al., 2002; Li et al., 2019; Pearce et al., 1992), so that high Hf/Sm and Zr/Sm ratios would reflect the infiltration of slab-derived amphibolite melts into the mantle source. La/Sm, by contrast, tracks solute-rich fluids released by melting of both the sediments and the amphiboliltized oceanic crust. Amphibole is the only mineral phase that fractionates Hf and Zr from Sm (Foley et al., 2002; Pearce et al., 1992). The scarcity of amphibole in mantle rocks from modern subduction zones cannot account for the compositional variations in Hf/Sm and Zr/Sm observed in the magmas (Pearce et al., 1992). As such, slab melting of altered oceanic crust in the amphibolite facies has been proposed as a cause of these variations, which is consistent with the observations of amphibolite melting in subducted slabs with a warm P-T path (Angiboust et al., 2017; Prigent et al., 2018). Below, we examine the composition of slab fluid markers in magmatism spanning the history of the IBM margin.

5.1- Large fluxes of water-rich slab fluids released during subduction infancy

The FABs possess a geochemical fingerprint in the markers of water-rich slab fluids that is intermediate between mid-ocean ridge basalts (MORBs) and back-arc basin basalts (BABBs) (Ba/Th = 63.26 – 92.47, Rb/Th = 5.50 – 39.54, Cs/Th = 0.05 – 0.54, H_2O/Ce = 484.06 – 2798.09; Table S1-4) (Fig. 4-5), indicating that a minor amount of slab fluid infiltrated the asthenospheric mantle during the first stages of subduction inception in IBM (Coulthard et al., 2021; Ishizuka et al., 2011b; Reagan et al., 2010; Reagan et al., 2017). There is an increase in the markers of slab dehydration from the FABs to the boninites (Ba/Th = 133.01 – 913.18, Rb/Th = 30.41 – 219.32, Cs/Th = 0.53 – 4.79 for the LSB glasses; and Ba/Th = 115.65 – 239.90, Rb/Th = 51.19 – 134.23, Cs/Th = 1.71-5.17 for the HSB glasses in Fig. 4-5; Table S1-4), that is associated with an increase in H_2O/Ce (Fig. 4A). The boninites also possess higher H_2O/Ce ratios (7522.55 – 21775.79) compared with the modern arc and the back-arc magmas. Although HSB have slightly higher markers of slab dehydration than LSB, their compositional ranges generally overlap (Fig. 4-5, 7). The sharp increase in the markers of slab dehydration (Rb/Th, Ba/Th, Cs/Th, Cs/Ba) from the FABs to the low-silica boninites further implies that large fluxes of water-rich fluids were released from the shallow part of the subducting slab (≤ 90 km slab depth) within ~1 Myr of subduction inception.

The high Th/Nb and La/Sm (Fig. 4, 6) in the IBM HSB further indicate that the subducted sediments began melting shortly after the subduction began. The high Hf/Sm and Zr/Sm in the IBM boninites (Fig. 6) has been proposed to track melting of the altered oceanic crust in the amphibolite facies, due to high temperatures on top of the nascent slab (Foley et al., 2002; Li et al., 2019; Pearce et al., 1992). Slab melting increases from the LSB to the HSB, as shown by the higher Hf/Sm and Zr/Sm ratios in the HSB (Fig. 6). Such high temperatures were perhaps caused by a return of asthenospheric mantle flow (Pearce and Robinson, 2010; Reagan et al., 2010), triggered by the sinking of the nascent subducted plate. Slab melting in

the amphibolite facies during the early stages of IBM reveals the warm thermal structure of the Pacific plate as it began sinking (Agard et al., 2020; Li et al., 2019; Prigent et al., 2018). As subduction matures, its slab thermal structure progressively cools over time (Holt and Condit, 2021).

5.2- Less water-rich slab fluids and more sediment melts released beneath the Mariana arc

The infant arc basalts possess an intermediate composition between arc and back-arc magmas in slab fluid proxies (Ba/Th = 57.93 – 299.23, Rb/Th = 9.29 – 34.43, Th/Nb = 0.08 – 0.87; Table S1-4) (light green compositional field Fig. 4) (Ribeiro et al., 2019). Their composition in these slab-fluid markers is generally much lower than that observed in the LSB and HSB (Fig. 4). During arc infancy, the slab fluids released from the slab at ~ 90 - 100 km depth progressively become less enriched in water and in sediment melt.

Mature arc basalts possess, instead, higher values for proxies of sediment melt (Th/Nb = 0.18 – 1.17) and water-rich fluids (Ba/Th = 138.18 – 1141.18, Rb/Th = 6.86 – 33.04, Cs/Th = 0.23 – 1.23, H_2O/Ce = 1727.82 – 9828.55; Table S1-5) than the infant arc magmas (Fig. 4-5). The slab fluids released at sub-arc depths (≥ 100 km depth) beneath the mature volcanic arc progressively became more aqueous and solute-rich, as compared to the fluids released beneath the infant arc. However, these deeper slab fluids generally remained much less aqueous than the shallow slab fluids released during subduction infancy (i.e., during boninitic magmatism). Thus, there is a rapid decrease in the water-rich and solute-rich slab fluids from the HSB to the infant arc magmas that occurred within 5 Myr of subduction inception (Fig. 6-7). As the volcanic arc began to develop, the slab capacity to transport water, Rb and Cs to depth diminished (Kessel et al., 2005; Manning, 2004; Schmidt and Poli, 1998); while sediment melting became more prevalent at sub-arc depth (Fig. 4B).

5.3- Slab fluid composition released beneath the SEMFR

The SEMFR magmas possess lower Hf/Sm and Zr/Sm ratios (Fig. 6) than the boninites, which suggests a cooler thermal structure on the mature subducted slab. Unlike the nascent slab, the Pacific slab subducting underneath the Southern Marianas did not permit melting of the oceanic crust in the amphibolite facies. The SEMFR basalts are however strongly enriched in markers of slab dehydration (Ba/Th= 93.86 – 798.36, Rb/Th = 9.51 – 139.75, Cs/Th = 0.22 – 17.79, H_2O/Ce = 1799.06 – 18935.56) (Fig. 4-5) compared to the Mariana arc magmas (Rb/Th ≤ 68, Cs/Th ≤ 4, H_2O/Ce ≤ 9829). The SEMFR basalts and associated olivine-hosted melt inclusions display similar enrichments in markers of water-rich slab fluids to those observed in the IBM boninites (Fig. 4-5). These results support the notion that the shallow part of the downgoing plate could extensively dehydrate within ~ 90 km from the trench (≤ 90 km depths to the slab) in cold subduction zones (Angiboust and Agard, 2010; Penniston-Dorland et al., 2015; Philippot, 1993; Ribeiro, 2022; Ribeiro et al., 2015). Shallow slab dehydration seems to be accompanied by a decoupling between Ba from Rb and Cs (as emphasized by the high Cs/Ba ratios of the SEMFR magmas and boninites in Fig. 4C), which may reveal differential partitioning into water-rich slab fluids with increasing slab depth (Bebout et al., 2007).

6- Origin of the slab fluids released in IBM since subduction inception

Pb-Sr radiogenic isotopes are commonly used to track the host reservoirs of the slab fluids in subduction zone magmas, as Pb and Sr are both mobilized with sediment melts and water-rich slab fluids (Kessel et al., 2005). Plotting markers of slab dehydration (Ba/Th) and sediment melting (Th/Nb) against Pb-Sr radiogenic isotopes can thus place additional constraints on how the sources of the slab fluids have varied throughout the lifetime of IBM

(Fig. 7-9). We also performed mixing calculations to assess the origin of the slab fluids and quantify the contribution of the host reservoirs (i.e., subducted serpentinized mantle, altered oceanic crust and sediments). Details about our mixing equations and end-member composition can be found in the supplementary material and in Table S2.

6.1- Sources of the water-rich slab fluids released at shallow slab depth (≤ 90 km)

Although subducted sediments are predicted to dehydrate first at shallow slab depths (≤ 90 km depths) (Rüpke et al., 2004; Schmidt and Poli, 1998), the composition of the water-rich slab fluids released from the sediments subducting underneath IBM may not account for the compositional variations observed in the IBM boninites (both LSB and HSB) and the SEMFR magmas. Indeed, the Ba, Cs, Rb do not seem to strongly partition into the water-rich fluids released during sediment dehydration (Johnson and Plank, 1999). Hence, the inferred compositions of sediment-derived, water-rich fluids possess much lower markers of slab dehydration (Rb/Th < 5, Ba/Th ≤ 100, Cs/Th < 1; see supplementary material and Table S2) than those observed in the boninites and SEMFR magmas (Ba/Th = 20.7 - 100.0, Rb/Th =1.7 – 12.4, Cs/Th = 0.15 – 0.39, $^{206}Pb/^{204}Pb$ = 19.03) (Fig. 4-5, 8-10). For instance, the inferred composition in Rb/Th and La/Sm of the sediment-derived, water-rich fluids cannot explain the compositional variations observed in the SEMFR magmas and IBM boninites (Fig. 4C). Retention of volatiles (H, C, N, S), alkalis (Rb, Cs) and other fluid-mobile elements (e.g., As, Sb) in the subducted sediments beyond ~40 km depth has also been observed in metasedimentary rocks from the Fransiscan complex and the Western Baja Terrane (Bebout et al., 2007; Sadofsky and Bebout, 2003). Such petrographic observations concur with the notion that the subducted sediments would retain most of their intra-slab, water-rich fluids to sub-arc depths to mainly contribute to the generation of arc magmas (Plank and Langmuir, 1993).

By contrast, Cs, Rb and Ba are easily partitioned into the water-rich fluids released during dehydration of the underlying serpentinized mantle and the altered oceanic crust from the subducting plate (Kessel et al., 2005; Scambelluri et al., 2001), so that their aqueous fluids would have elevated Ba/Th, Cs/Th and Rb/Th ratios (Fig. 4-5, 8-10 and supplementary material). Their dehydration could account for the compositional variations observed in the IBM boninites, SEMFR basalts and associated olivine-hosted melt inclusions (Fig. 4-5). Petrographic observations of cold subducting slabs (e.g., Western Alps and Zagros) and modeled thermal structure of nascent slabs also suggest that the subducted oceanic crust and the underlying serpentinized mantle are the main sources of water-rich slab fluids released at shallow depths (≤ 90 km) (Angiboust et al., 2012; Holt and Condit, 2021; Muñoz-Montecinos et al., 2021). They would release large fluxes of water-rich slab fluids beneath the fore-arc as pulses from ~ 50 – 80 km the trench (Holt and Condit, 2021) within 2 to 5 Myr of subduction inception, as evidenced by the elevated markers of slab dehydration in the boninites (Fig. 6).

6.2- A temporal evolution in the fluid reservoirs throughout the lifetime of IBM

The composition of the IBM magmas suggests a temporal change in the slab fluids compositions that was associated with a change in their host reservoirs and increasing slab depth (Fig. 6-10). This temporal evolution in magma composition, as highlighted in the figures (Fig. 3, 6-10) by white numbers in black circles, is described as follows:

1- Formation of the FABs by near-trench spreading from 48 to 52 Myr (Ishizuka et al., 2006; Reagan et al., 2019; Reagan et al., 2017). Limited slab fluids infiltrated the relatively fertile asthenospheric mantle, which has a depleted MORB-like mantle

425 (DMM) composition (Fig. 4-6, 8-10). The low values of slab-fluid proxies suggest
426 that the nascent subducted Pacific slab dehydrated relatively little during subduction
427 inception (Coulthard et al., 2021; Reagan et al., 2019; Reagan et al., 2010).
428
429 2- Formation of the LSB by near-trench spreading from 48 to 50 Myr (Coulthard
430 et al., 2021; Reagan et al., 2019; Reagan et al., 2010). Water-rich and solute-rich slab
431 fluids progressively infiltrated the asthenospheric mantle residual to FAB melting, to
432 produce the LSB (Ishizuka et al., 2006; Reagan et al., 2019; Reagan et al., 2017). The
433 LSB marks the transition from adiabatic decompression melting to fluid-assisted
434 mantle melting (Coulthard et al., 2021; Reagan et al., 2019; Reagan et al., 2017;
435 Shervais et al., 2019). The $^{86}Sr/^{87}Sr$ isotopic composition of the LSB ($^{86}Sr/^{87}Sr <$
436 0.704) is lower than that of the HSB ($^{86}Sr/^{87}Sr > 0.704$), and is best explained by the
437 infiltration of water-rich fluids released from dehydrating of subducted crust and
438 serpentinized mantle into their mantle source (Fig. 8B). $^{208}Pb/^{204}Pb$ vs. $^{206}Pb/^{204}Pb$
439 variations (Fig. 10A) further suggest that there is a negligible contribution from the
440 subducted sediments in the LSB, and that altered oceanic crust dominates the
441 composition of the first fluids released from the nascent slab (Li et al., 2019). Our
442 mixing calculations suggest that the water-rich fluids released during the early stages
443 of IBM mainly come from dehydrating 50 – 100 % of the altered oceanic crust, and 0
444 - 50% of the serpentinized mantle. Up to 85 % of this water-rich slab fluid infiltrated
445 residual proto-arc mantle to produce the LSB (Fig. 8, 10). Deserpentinization of the
446 subducted mantle likely triggered dehydration and melting of the altered oceanic crust
447 in the amphibolite facies at shallow slab depth (< 100 km depth) (Fig. 6). The absence
448 of sediment fingerprint in the Pb isotopic composition of the LSB suggests that the

449 sediments were not subducted; and they were instead accreted or relatively limited
450 during the early stages of IBM (Li et al., 2019).
451
452 3- Formation of the HSB by fluid-assisted melting of the proto-arc mantle,
453 residual from LSB melting, from 45 to 50 Myr (Ishizuka et al., 2006; Reagan et al.,
454 2017). In contrast to the LSB, the Sr isotopic composition of the altered oceanic crust
455 cannot account for the Sr isotopic composition of the HSB, as the isotopic
456 composition of the oceanic crust in $^{87}Sr/^{86}Sr$ (0.7045) is too low (Fig. 8B). Instead,
457 the HSB are best explained by the infiltration of a water-rich fluid that was released
458 from dehydrating at least 50% subducted serpentinized mantle and up to ~50%
459 sediments. Up to 60% of this composite fluid was captured by the HSB. These results
460 further suggest that the sediments began to be subducted within 2 – 3 Myr of
461 subduction inception. The Pb isotopic composition of the HSB (Fig. 8A, 10A-B) also
462 requires the involvement of a fluid from the altered oceanic crust, either as a water-
463 rich slab fluid or a solute-rich fluid. Variations in $^{206}Pb/^{204}Pb$ vs. Ba/Th (Fig. 8A)
464 further suggests that at least 50% altered oceanic crust and less than 50%
465 serpentinized mantle is required to account for the compositional variations observed
466 in the HSB. Hence, the composition of the HSB is best explained by the infiltration of
467 water-rich slab fluids that were released from dehydrating altered oceanic crust (50 -
468 100%), the subducted serpentinized mantle (≤ 50%) and the subducted sediments (≤
469 50%). Up to 60 to 85% of this water-rich slab fluid was captured by the HSB (Fig. 8,
470 10).
471 The solute-rich fluids captured by the HSB come from melting the oceanic
472 crust in the amphibolite facies (Fig. 6) (Li et al., 2019) and the subducted sediments
473 (Fig. 8C). Up to 35% of sediment melt infiltrated the proto-arc mantle. The

compositional variations in Th/Nb vs. $^{206}Pb/^{204}Pb$ of the HSB requires, however, an end-member with high Th/Nb ratio (~1-3) and lower Pb isotopic composition ($^{206}Pb/^{204}Pb$ ~18.5) than the Pacific sediments drilled at ODP Leg 129, Site 800 (Fig. 8C) (Plank and Langmuir, 1998). Such observations imply that the composition of the Pacific sediments that subducted underneath IBM ~50 Myr ago might have been much less radiogenic than are the sediments of ODP Site 800. Melting of the subducted sediments triggered by dehydration of the subducted mantle offers a simple alternative to that scenario. The resulting slab fluids would have had a Pb isotopic composition (~18.5) intermediate between that of the sediment and the serpentinized mantle.

Deserpentinization of the subducted mantle at shallow slab depths (< 100 km) likely triggered dehydration and melting of the altered oceanic crust and the subducted sediments, which facilitated melting of the residual, proto-arc mantle. Hence, the sediments are progressively incorporated into the subducted slab through time, as a mélange zone overlying the slab interface (Bebout, 2007; Cloos and Shreve, 1988; Marschall and Schumacher, 2012) within ~ 1-2 Myr after subduction inception (Li et al., 2019). Magma composition suggests that the sediment contribution increased from the LSB to the HSB; while the contribution of the altered oceanic crust decreased over time. The decreasing capacity in dehydrating the subducted oceanic crust might indicate progressive slab eclogitisation at ~ 90 km depths. This temporal change in the host reservoirs from the LSB to the HSB could reflect a deepening of magma generation. The higher K_2O content of the HSB, as compared to FABs and LSB (Fig. 3A), suggests that the HSB overlaid a deeper portion of the subducted slab. Deepening of magma generation in the HSB could be

498 associated to a slab rollback and/or to a retreat of the melting front (Fig. 11) (Ishizuka
499 et al., 2006; Reagan et al., 2019; Reagan et al., 2010; Stern and Bloomer, 1992).
500
501 4- The infant arc began to develop at ~ 41 to 45 Myr, forming small trails of
502 subaerial and submarine volcanic cones within 90 km from the trench (Ishizuka et al.,
503 2011a; Kanayama et al., 2012, 2014). Infant arc magmas formed by melting of a
504 relatively fertile asthenosphere (Nb/Yb ~ 1 and TiO_2 > 0.4) that was infiltrated by
505 water-rich slab fluids and solute-rich melts. The sub-arc mantle was likely
506 replenished by the inflow of fresh asthenosphere. Variations in Ba/Th, $^{206}Pb/^{204}Pb$ and
507 $^{86}Sr/^{87}Sr$ suggest that the infant arc magmas captured the water-rich slab fluids
508 released from dehydrating 0-50% subducted mantle and 50-100% altered oceanic
509 crust; and 40-50% of this water-rich slab fluids infiltrated the sub-arc mantle (Fig.
510 8A). Variations in $^{208}Pb/^{204}Pb$ and $^{206}Pb/^{204}Pb$ further suggest that the subducted
511 sediments could also contribute to fingerprint the Pb isotopic composition of the
512 infant arc magmas, as depicted by a light green compositional field in Fig. 10A.
513 Hence, the subducted sediments could also dehydrate to some extent in the early arc,
514 as suggested by the variations in $^{86}Sr/^{87}Sr$ vs. Ba/Th (Fig. 8B). During that stage,
515 melting of the oceanic crust was negligible, so that the solute-rich fluids mostly
516 derived from sediment melting. The infant arc magmas captured the sediment melts
517 with a similar Pb isotopic composition to that observed in the HSB. 35% of sediment
518 melt was captured by the infant arc magmas (Fig. 8C).
519
520 5- The mature volcanic arc front began to develop ~ 40 – 42 Myr by fluid-assisted
521 melting of a relatively undepleted sub-arc mantle, forming larger and thicker-crust
522 volcanoes (Ishizuka et al., 2011b). The arc magmas captured the slab fluids released

523 from the deeper part of the subducted slab (~ 100 – 150 km depth), so that sediment
524 melting was more prevalent in the mature arc (Fig. 8C). The Pb-Sr isotopic
525 compositions of mature arc magmas suggest that the water-rich slab fluids were
526 released from dehydrating 50 - 100% altered oceanic crust, and 0 - 50% subducted
527 mantle, with a minor contribution from the sediments (Fig. 8A-B). However,
528 variations in Ba/Th and $^{206}Pb/^{204}Pb$ are best explained by mixing between 50% altered
529 oceanic crust and 50% subducted mantle (Fig. 8B). The solute-rich melts only came
530 from melting of the sediments (Fig. 8C). The mature arc magmas captured up to 40 %
531 of water-rich slab fluid and up to 70% of sediment melt. The contribution of the
532 solute-rich fluids released from the subducted sediments is much clearer in the mature
533 arc magmas (Fig. 4C, 8C) (Elliott, 2003; Johnson and Plank, 1999; Pearce et al.,
534 2005), implying that sediment melting become more prevalent at sub-arc depth.
535 Dehydration of the subducted serpentinized mantle triggered dehydration and melting
536 of the overlying sediments, and dehydration of the altered oceanic crust (Klaver et al.,
537 2020).
538 The temporal change in slab-fluid reservoirs is likely associated with the
539 retreat of the volcanic arc front and a deepening of magma generation with time (Fig.
540 11). Arc migration is likely associated with serpentinization and cooling of the fore-
541 arc mantle, which progressively displaces the depth of magma generation until it
542 stabilizes in its current location (i.e., ~ 100 – 150 km from the trench and ~ 100 km
543 depth to the slab) (Ribeiro et al., 2019). Hence, serpentinization of the fore-arc mantle
544 could be essential in the development of a long-lived subduction zone (Agard et al.,
545 2020; Gerya et al., 2008; Hyndman and Peacock, 2003; Ribeiro and Lee, 2017;
546 Ribeiro et al., 2019). It would permit the formation of a subduction channel (Cloos
547 and Shreve, 1988), which could act as a lubricating layer on top of the subducted slab

548 that would facilitate deeper slab penetration and subduction stabilization (Agard et al.,
549 2020; Gerya et al., 2008).
550
551 **6.3- Comparison with the SEMFR magmas: Implications for the formation of the**
552 **IBM proto-arc crust**
553 The SEMFR magmas formed by near-trench spreading above a long-lived subduction
554 zone (Ribeiro et al., 2013a). The basalts possess similar chemical features to the FABs in
555 major element contents and in some of the trace element contents. However, unlike the
556 FABs, the SEMFR basalts captured greater extent of slab fluids. The SEMFR olivine-hosted
557 melt inclusions display similar features to the LSB in terms of major and trace element
558 contents, implying that they formed under similar (but not identical) petrogenetic conditions
559 (Fig. 3-4). The SEMFR basalts (bulk rock) display similar Pb-Sr isotopic composition to the
560 LSB (Fig. 9-10), which support the notion that they incorporated the slab fluids that were
561 released from the shallow part of the subducted slab (Ribeiro et al., 2013b). The water-rich
562 slab fluid was released from dehydrating at least 50% of the altered oceanic crust, less than
563 50% of subducted mantle (Fig. 9A-B). The SEMFR magmas captured 40% to 80% of this
564 water-rich slab fluids. Although sediments are subducted in the Southern Mariana Trench, the
565 SEMFR magmas possess similar Pb-Sr isotopic composition to that of the LSB (Fig. 8-10),
566 implying that the subducting sediments would retain most of their volatiles and alkalis to
567 release them at sub-arc depth. Hence, the subducting altered oceanic crust and the underlying
568 serpentinized mantle represent the main sources of water-rich slab fluids released beneath the
569 IBM fore-arc.
570 The strong enrichment in markers of water-rich slab fluids in the SEMFR glasses (Fig. 4-
571 6) further suggest that extensive slab dehydration could occur within ~ 90 km from the trench
572 both in mature (i.e., in the fore-arc) subduction zones (Ribeiro et al., 2015). Dehydration of
573 the subducted mantle and the altered oceanic crust likely dominates the water-rich slab fluids

574 released at shallow slab depths. Dehydration and melting of the subducted sediments become
575 more prevalent beneath the volcanic arc front (Johnson and Plank, 1999; Plank, 2005; Plank
576 and Langmuir, 1993, 1998). The sediments would thus retain most of their alkalis and some
577 of their volatiles to sub-arc depth to contribute to arc magma generation (Bebout et al., 2007;
578 Bebout et al., 1999; Busigny et al., 2003).

579 The fact that the SEMFR magmas display similar geochemical fingerprint to the IBM
580 proto-arc magmas further indicates that, despite having developed above a long-lived
581 subduction zone, the SEMFR can place important new constraints onto the processes that
582 occurred at the onset of a subduction zone. This is particularly important because there are a
583 few modern analogs to subduction infancy. These similarities further suggest that the IBM
584 proto-arc crust formed within 90 km from the trench and overlain a nascent slab at $\leq$ 90 km
585 depth or less. Such findings are consistent with the current location of the proto-arc crust that
586 has been preserved in the Bonin Island (Fig. 2) (Kanayama et al., 2012, 2014).

587

588 **7- Conclusions**

589 The composition slab-derived water-rich and solute-rich fluids evolved over the
590 lifetime of IBM (~ 52 Myr ago), reflecting a change in the sources of these fluids with time.
591 Markers of high slab dehydration (e.g., elevated Ba/Th, Rb/Th, Cs/Th, H_2O/Ce) recorded in
592 the IBM boninites indicate that large fluxes of water-rich slab fluids were mainly released
593 from dehydrating the subducted serpentinized mantle and from the altered oceanic crust
594 within 90 km from trench ($\leq$ 90 km slab depth). As the subduction evolves, less water-rich
595 slab fluids are released from dehydrating the subducted serpentinized mantle and the altered
596 oceanic crust to sub-arc depths. The contribution from sediments, as water-rich and solute-
597 rich fluids, initiated later and hence deeper, suggesting that the sediments overlying the
598 Pacific plate were not subducted until ~ 50 Myr.

Changes in slab fluid compositions and in their sources reveal retreat of the volcanic arc front, so that mature arc magmas captured slab fluids that are released from a deeper part of the slab where sediment melting can occur. Therefore, mature arc magmas formed deeper and they captured less water-rich slab fluids, compared to the shallow slab fluids released during subduction infancy. Arc retreat and subduction stabilization in IBM were likely modulated by the growth of the serpentinized fore-arc mantle, which could, therefore play a key role in long-lived oceanic subduction zones. However, there is not a single scenario of magma petrogenesis. Magma compositions depend upon the tectonic conditions, the thermal structure of the subducted plate, and the mantle flow regime that prevail during subduction evolution.

Acknowledgements

JR thanks Robert Stern (UTD), Julian Pearce (Cardiff University), Mark Reagan (Iowa University), Jim Gill (University of California in Santa Cruz), Adam Kent (Oregon State University), Susanne Straub (LDEO), Osamu Ishizuka and Yoshihiko Tamura (both at JAMSTEC) for discussions that have inspired this manuscript over the past few years. Two anonymous reviewers and Catherine Chauvel, the editor, are thanked for insightful comments. JR acknowledge a PIFI fellowship n° 2020VCB000.

References

Agard, P., Prigent, C., Soret, M., Dubacq, B., Guillot, S., and Deldicque, D., 2020, Slabitization: Mechanisms controlling subduction development and viscous coupling: Earth-Science Reviews, v. 208, p. 103259.

Angiboust, S., and Agard, P., 2010, Initial water budget: The key to detaching large volumes of eclogitized oceanic crust along the subduction channel?: Lithos, v. 120, no. 3, p. 453-474.

Angiboust, S., Hyppolito, T., Glodny, J., Cambeses, A., Garcia-Casco, A., Calderón, M., and Juliani, C., 2017, Hot subduction in the middle Jurassic and partial melting of oceanic crust in Chilean Patagonia: Gondwana Research, v. 42, p. 104-125.

628 Angiboust, S., Wolf, S., Burov, E., Agard, P., and Yamato, P., 2012, Effect of fluid circulation
629 on subduction interface tectonic processes: Insights from thermo-mechanical
630 numerical modelling: Earth and Planetary Science Letters, v. 357-358, p. 238-248.
631 Baker, E. T., Embley, R. W., Walker, S. L., Resing, J. A., Lupton, J. E., Nakamura, K.-i., de
632 Ronde, C. E. J., and Massoth, G. J., 2008, Hydrothermal activity and volcano
633 distribution along the Mariana arc: Journal of Geophysical Research, v. 113, no. B8,
634 p. B08S09, DOI: 10.1029/2005GC000948.
635 Bebout, G. E., 2007, Metamorphic chemical geodynamics of subduction zones: Earth and
636 Planetary Science Letters, v. 260, no. 3–4, p. 373-393.
637 Bebout, G. E., Bebout, A. E., and Graham, C. M., 2007, Cycling of B, Li, and LILE (K, Cs, Rb, Ba,
638 Sr) into subduction zones: SIMS evidence from micas in high-P/T metasedimentary
639 rocks: Chemical Geology, v. 239, no. 3, p. 284-304.
640 Bebout, G. E., Ryan, J. G., Leeman, W. P., and Bebout, A. E., 1999, Fractionation of trace
641 elements by subduction-zone metamorphism — effect of convergent-margin
642 thermal evolution: Earth and Planetary Science Letters, v. 171, no. 1, p. 63-81.
643 Brounce, M. N., Kelley, K. A., Stern, R. J., Martinez, F., and Cottrell, E., 2016, The Fina Nagu
644 Volcanic Complex: Unusual submarine arc volcanism in the rapidly deforming
645 southern Mariana margin: Geochemistry Geophysics Geosystems, v. 17, p. 4078–
646 4091, doi:4010.1002/2016GC006457.
647 Busigny, V., Cartigny, P., Philippot, P., Ader, M., and Javoy, M., 2003, Massive recycling of
648 nitrogen and other fluid-mobile elements (K, Rb, Cs, H) in a cold slab environment:
649 evidence from HP to UHP oceanic metasediments of the Schistes Lustrés nappe
650 (western Alps, Europe): Earth and Planetary Science Letters, v. 215, no. 1, p. 27-42.
651 Cloos, M., and Shreve, R. L., 1988, Subduction-channel model of prism accretion, melange
652 formation, sediment subduction, and subduction erosion at convergent plate
653 margins: 1. Background and description: pure and applied geophysics, v. 128, no. 3,
654 p. 455-500.
655 Coulthard, D. A. J., Reagan, M. K., Shimizu, K., Bindeman, I. N., Brounce, M., Almeev, R. R.,
656 Ryan, J. G., Chapman, T., Shervais, J., and Pearce, J. A., 2021, Magma source
657 evolution following subduction initiation: Evidence from the element concentrations,
658 stable isotope ratios, and water contents of volcanic glasses from the Bonin forearc
659 (IODP Expedition 352): Geochemistry Geophysics Geosystems, v. 22, p.
660 e2020GC009054, https://doi.org/009010.001029/002020GC009054.
661 Dixon, J. E., Bindeman, I. N., Kingsley, R. H., Simons, K. K., Le Roux, P. J., Hajewski, T. R.,
662 Swart, P., Langmuir, C. H., Ryan, J. G., Walowski, K. J., Wada, I., and Wallace, P. J.,
663 2017, Light Stable Isotopic Compositions of Enriched Mantle Sources: Resolving the
664 Dehydration Paradox: Geochemistry, Geophysics, Geosystems, v. 18, no. 11, p. 3801-
665 3839.
666 Dixon, J. E., Leist, L., Langmuir, C. H., and Schilling, J.-G., 2002, Recycled dehydrated
667 lithosphere observed in plume-influenced mid-ocean-ridge basalt: Nature, v. 420,
668 no. 6914, p. 385-389.
669 Elliott, T. R., 2003, Tracers of the slab, *in* Eiler, J., ed., Inside the Subduction Factory, Volume
670 138: Washington, DC, Geophysical Monograph Series, p. 23-45.
671 Elliott, T. R., Plank, T., Zindler, A., White, W., and Bourdon, B., 1997, Element transport from
672 slab to volcanic front at the Mariana arc: Journal of Geophysical Research, v. B102, p.
673 14991-15019.

674 Foley, S., Tiepolo, M., and Vannucci, R., 2002, Growth of early continental crust controlled
675 by melting of amphibolite in subduction zones: Nature, v. 417, no. 6891, p. 837-840.
676 Gaetani, G. A., O'Leary, J. A., Shimizu, N., Bucholz, C. E., and Newville, M., 2012, Rapid
677 reequilibration of H2O and oxygen fugacity in olivine-hosted melt inclusions:
678 Geology, v. 40, no. 10, p. 915-918.
679 Gerya, T. V., Connolly, J. A. D., and Yuen, D. A., 2008, Why is terrestrial subduction one-
680 sided?: Geology, v. 36, no. 1, p. 43-46.
681 Grove, T. L., Chatterjee, N., Parman, S. W., and Médard, E., 2006, The influence of H2O on
682 mantle wedge melting: Earth and Planetary Science Letters, v. 249, no. 1–2, p. 74-89.
683 Hatherton, T., and Dickinson, W. R., 1969, The relationship between andesitic volcanism and
684 seismicity in Indonesia, the Lesser Antilles, and other island arcs: Journal of
685 Geophysical Research (1896-1977), v. 74, no. 22, p. 5301-5310.
686 Holt, A., and Condit, C. B., 2021, Slab temperature evolution over the lifetime of a
687 subduction zone: Geochemistry, Geophysics, Geosystems, v. 22, no. 6, p.
688 e2020GC009476, https://doi.org/009410.001029/002020GC009476.
689 Hyndman, R. D., and Peacock, S. M., 2003, Serpentinization of the forearc mantle: Earth and
690 Planetary Science Letters, v. 212, no. 3–4, p. 417-432.
691 Ishizuka, O., Kimura, J.-I., Li, Y. B., Stern, R. J., Reagan, M. K., Taylor, R. N., Ohara, Y.,
692 Bloomer, S. H., Ishii, T., Hargrove Iii, U. S., and Haraguchi, S., 2006, Early stages in the
693 evolution of Izu–Bonin arc volcanism: New age, chemical, and isotopic constraints:
694 Earth and Planetary Science Letters, v. 250, no. 1–2, p. 385-401.
695 Ishizuka, O., Tani, K., Reagan, M. K., Kanayama, K., Umino, S., Harigane, Y., Sakamoto, I.,
696 Miyajima, Y., Yuasa, M., and Dunkley, D. J., 2011a, The timescales of subduction
697 initiation and subsequent evolution of an oceanic island arc: Earth and Planetary
698 Science Letters, v. 306, no. 3, p. 229-240.
699 Ishizuka, O., Taylor, R. N., Umino, S., and Kanayama, K., 2020, Geochemical Evolution of Arc
700 and Slab Following Subduction Initiation: a Record from the Bonin Islands, Japan:
701 Journal of Petrology, v. 61, no. 5.
702 Ishizuka, O., Taylor, R. N., Yuasa, M., and Ohara, Y., 2011b, Making and breaking an island
703 arc: A new perspective from the Oligocene Kyushu‐Palau arc, Philippine Sea:
704 Geochemistry Geophysics Geosystems, v. 12, no. 5.
705 Johnson, M. C., and Plank, T., 1999, Dehydration and melting experiments constrain the fate
706 of subducted sediments: Geochemistry Geophysics Geosystems, v. 1, p. 1007, DOI:
707 1010.1029/1999GC000014.
708 Kanayama, K., Umino, S., and Ishizuka, O., 2012, Eocene volcanism during the incipient stage
709 of Izu–Ogasawara Arc: Geology and petrology of the Mukojima Island Group, the
710 Ogasawara Islands: Island Arc, v. 21, no. 4, p. 288-316.
711 -, 2014, Shallow submarine volcano group in the early stage of island arc development:
712 Geology and petrology of small islands south off Hahajima main island, the
713 Ogasawara Islands: Journal of Asian Earth Sciences, v. 85, p. 1-25.
714 Kelley, K. A., Plank, T., Ludden, J. N., and Staudigel, H., 2003, Composition of altered oceanic
715 crust at ODP Sites 801 and 1149: Geochem. Geophys. Geosyst., v. 4, no. 6, p. 8910,
716 DOI: 8910.1029/2002GC000435.
717 Kent, A. J. R., Norman, M. D., Hutcheon, I. D., and Stolper, E. M., 1999, Assimilation of
718 seawater-derived components in an oceanic volcano: evidence from matrix glasses
719 and glass inclusions from Loihi seamount, Hawaii: Chemical Geology, v. 156, no. 1–4,
720 p. 299-319.

721 Kessel, R., Schmidt, M. W., Ulmer, P., and Pettke, T., 2005, Trace element signature of
722 subduction-zone fluids, melts and supercritical liquids at 120–180 km depth: Nature,
723 v. 437, p. 724-727.
724 Kimura, J.-I., and Stern, R. J., 2008, Neogene volcanism of the Japan island arc: The K-h
725 relationship revisited, *in* Spencer, J. E., and Titley, S. R., eds., Ores and orogenesis:
726 Circum-Pacific tectonics, geologic evolution, and ore deposits, Volume 22: Arizona,
727 Arizona Geological Society Digest, p. 187-202.
728 Klaver, M., Lewis, J. F., Parkinson, I. J., Elburg, M. A., Vroon, P. Z., Kelley, K. A., and Elliott, T.
729 R., 2020, Sr isotopes in arcs revisited: tracking slab dehydration using δ 88/86Sr and
730 87Sr/86Sr systematics of arc lavas: Geochimica et Cosmochimica Acta, v. 288, p. 101-
731 119.
732 Kogiso, T., Tatsumi, Y., and Nakano, S., 1997, Trace element transport during dehydration
733 processes in the subducted oceanic crust: 1. Experiments and implications for the
734 origin of ocean island basalts: Earth and Planetary Science Letters, v. 148, no. 1–2, p.
735 193-205.
736 Li, H. Y., Taylor, R. N., Prytulak, J., Kirchenbaur, M., Shervais, J. W., Ryan, J. G., Godard, M.,
737 Reagan, M. K., and Pearce, J. A., 2019, Radiogenic isotopes document the start of
738 subduction in the Western Pacific: Earth and Planetary Science Letters, v. 518, p.
739 197-210.
740 Manning, C. E., 2004, The chemistry of subduction-zone fluids: Earth and Planetary Science
741 Letters, v. 223, no. 1-2, p. 1-16.
742 Marschall, H. R., and Schumacher, J., 2012, Arc magmas sourced from mélange diapirs in
743 subduction zones: Nature Geoscience, v. 5, no. 12, p. 862-867.
744 Martinez, F., Fryer, P., and Becker, N., 2000, Geophysical characteristics of the southern
745 Mariana Trough, 11°50'N-13°40'N: Journal of Geophysical Research, v. 105, no. B7, p.
746 16,591-516,607.
747 Martinez, F., Stern, R. J., Kelley, K., Ohara, Y., Sleeper, J. D., Ribeiro, J., and Brounce, M.,
748 2018, Diffuse extension of the southern Mariana margin: implications for subduction
749 zone infancy and plate tectonics: Journal of Geophysical Research, v. 123, p. 892–
750 916, https://doi.org/810.1002/2017JB014684.
751 Maunder, B., Prytulak, J., Goes, S., and Reagan, M., 2020, Rapid subduction initiation and
752 magmatism in the Western Pacific driven by internal vertical forces: Nature
753 Communications, v. 11, no. 1, p. 1874.
754 McCulloch, M. T., and Gamble, J. A., 1991, Geochemical and geodynamical constraints on
755 subduction zone magmatism: Earth and Planetary Science Letters, v. 102, no. 3–4, p.
756 358-374.
757 Michibayashi, K., Ohara, Y., Stern, R. J., Fryer, P., Kimura, J.-I., Tasaka, M., Harigane, Y., and
758 Ishii, T., 2009, Peridotites from a ductile shear zone within back-arc lithospheric
759 mantle, southern Mariana Trench: Results of a Shinkai 6500 dive: Geochemistry
760 Geophysics Geosystems, v. 10, no. 5, p. Q05X06, DOI: 10.1029/2008GC002197.
761 Muñoz-Montecinos, J., Angiboust, S., Garcia-Casco, A., Glodny, J., and Bebout, G. E., 2021,
762 Episodic hydrofracturing and large-scale flushing along deep subduction interfaces:
763 Implications for fluid transfer and carbon recycling (Zagros Orogen, southeastern
764 Iran): Chemical Geology, v. 571, p. 120173.
765 Ohara, Y., and Ishii, T., 1998, Peridotites from the southern Mariana forearc: Heterogeneous
766 fluid supply in mantle wedge: Island Arc, v. 7, no. 3, p. 541-558.

767 Pearce, J. A., Lippard, S. J., and Roberts, S., 1984, Characteristics and tectonic significance of
768 supra-subduction zone ophiolites: Geological Society, London, Special Publications,
769 v. 16, no. 1, p. 77-94.
770 Pearce, J. A., and Reagan, M. K., 2019, Identification, classification, and interpretation of
771 boninites from Anthropocene to Eoarchean using Si-Mg-Ti systematics: Geological
772 Society of America Bulletin, v. 15, no. 4, p. 1008-1037,
773 https://doi.org/1010.1130/GES01661.01661.
774 Pearce, J. A., and Robinson, P. T., 2010, The Troodos ophiolitic complex probably formed in a
775 subduction initiation, slab edge setting: Gondwana Research, v. 18, no. 1, p. 60-81.
776 Pearce, J. A., Stern, R. J., Bloomer, S. H., and Fryer, P., 2005, Geochemical mapping of the
777 Mariana arc-basin system : Implications for the nature and distribution of subduction
778 components: Geochemistry Geophysics Geosystems, v. 6, no. 7, p. Q07006,
779 DOI:07010.01029/02004GC000895.
780 Pearce, J. A., Thirlwall, M. F., Ingram, G., Murton, B. J., Arculus, R. J., and Van der Laan, S. R.,
781 1992, Isotopic evidence for the origin of boninites and related rocks drilled in the Izu-
782 Bonin (Ogasawara) forearc, Leg 125, *in* Fryer, P., Pearce, J. A., and Stokking, L., et al.,
783 eds., Proceedings of the Ocean Drilling Program, Scientific Results 125, Volume 125:
784 Texas A&M University, Austin, Tx, IODP, p. 237-261,
785 http://dx.doi.org/210.2973/odp.proc.sr.2125.2134.1992.
786 Peccerillo, A., and Taylor, S. R., 1976, Geochemistry of Eocene calcalkaline volcanic rocks
787 from the Kastamonu Area, Northern Turkey: Contribution to Mineralogy and
788 Petrology, v. 58, p. 63-81.
789 Penniston-Dorland, S. C., Kohn, M. J., and Manning, C. E., 2015, The global range of
790 subduction zone thermal structures from exhumed blueschists and eclogites: Rocks
791 are hotter than models: Earth and Planetary Science Letters, v. 428, p. 243-254.
792 Philippot, P., 1993, Fluid-melt-rock interaction in mafic eclogites and coesite-bearing
793 metasediments: Constraints on volatile recycling during subduction: Chemical
794 Geology, v. 108, no. 1, p. 93-112.
795 Plank, T., 2005, Constraints from Thorium/Lanthanum on Sediment Recycling at Subduction
796 Zones and the Evolution of the Continents: Journal of petrology, v. 46, no. 5, p. 921-
797 944.
798 Plank, T., and Langmuir, C. H., 1993, Tracing trace elements from sediment input to volcanic
799 output at subduction zones: Nature, v. 362, no. 6422, p. 739-743.
800 -, 1998, The chemical composition of subducting sediment and its consequences for the
801 crust and mantle: Chemical Geology, v. 145, no. 3-4, p. 325-394.
802 Prigent, C., Guillot, S., Agard, P., Lemarchand, D., Soret, M., and Ulrich, M., 2018, Transfer of
803 subduction fluids into the deforming mantle wedge during nascent subduction:
804 Evidence from trace elements and boron isotopes (Semail ophiolite, Oman): Earth
805 and Planetary Science Letters, v. 484, p. 213-228.
806 Reagan, M. K., Heaton, D. E., Schmitz, M. D., Pearce, J. A., Shervais, J. W., and Koppers, A. A.
807 P., 2019, Forearc ages reveal extensive short-lived and rapid seafloor spreading
808 following subduction initiation: Earth and Planetary Science Letters, v. 506, p. 520-
809 529.
810 Reagan, M. K., Ishizuka, O., Stern, R. J., Kelley, K. A., Ohara, Y., Blichert-Toft, J., Bloomer, S.
811 H., Cash, J., Fryer, P., Hanan, B. B., Hickey-Vargas, R., Ishii, T., Kimura, J.-I., Peate, D.
812 W., Rowe, M. C., and Woods, M., 2010, Fore-arc basalts and subduction initiation in

the Izu-Bonin-Mariana system: Geochemistry Geophysics Geosystems, v. 11, no. 3, p. Q03X12, DOI: 10.1029/2009GC002871.

Reagan, M. K., Pearce, J. A., Petronotis, K., Almeev, R. R., Avery, A. J., Carvallo, C., Chapman, T., Christeson, G. L., Ferré, E. C., Godard, M., Heaton, D. E., Kirchenbaur, M., Kurz, W., Kutterolf, S., Li, H., Li, Y., Michibayashi, K., Morgan, S., Nelson, W. R., Prytulak, J., Python, M., Robertson, A. H. F., Ryan, J. G., Sager, W. W., Sakuyama, T., Shervais, J. W., Shimizu, K., and Whattam, S. A., 2017, Subduction initiation and ophiolite crust: new insights from IODP drilling: International Geology Review, v. 59, no. 11, p. 1439-1450.

Ribeiro, J., 2022, Slab dehydration beneath forearcs: Insights from the southern Mariana and Matthew-Hunter rifts: Geochemical Perspective Letters, v. 20, p. 22–26, doi: 10.7185/geochemlet.2203.

Ribeiro, J., and Lee, C. T. A., 2017, An imbalance in the deep water cycle at subduction zones: The potential importance of the fore-arc mantle: Earth and Planetary Science Letters, v. 479, p. 298-309, https://doi.org/210.1016/j.epsl.2017.1009.1018.

Ribeiro, J., Stern, R. J., Martinez, F., Ishizuka, O., Merle, S. G., Kelley, K. A., Anthony, E. Y., Ren, M., Ohara, Y., Reagan, M., Girard, G., and Bloomer, S. H., 2013a, Geodynamic evolution of a forearc rift in the southernmost Mariana Arc: Island Arc, v. 22, p. 453-476.

Ribeiro, J. M., Ishizuka, O., Lee, C. T. A., and Girard, G., 2019, Evolution and maturation of the nascent Mariana arc: Earth and Planetary Science Letters, v. 530, no. 115912, p. https://doi.org/10.1016/j.epsl.2019.115912.

Ribeiro, J. M., Stern, R. J., Kelley, K., Shaw, A., Martinez, F., and Ohara, Y., 2015, Composition of the slab-derived fluids released beneath the Mariana forearc: evidence for shallow dehydration of the subducting plate: Earth and Planetary Science Letters, v. 418, p. 136–148, doi: 110.1016/j.epsl.2015.1002.1018.

Ribeiro, J. M., Stern, R. J., Kelley, K. A., Martinez, F., Ishizuka, O., Manton, W. I., and Ohara, Y., 2013b, Nature and distribution of slab-derived fluids and mantle sources beneath the Southeast Mariana forearc rift: Geochemistry, Geophysics, Geosystems, v. 14, no. 10, p. 4585-4607.

Rüpke, L. H., Morgan, J. P., Hort, M., and Connolly, J. A. D., 2004, Serpentine and the subduction zone water cycle: Earth and Planetary Science Letters, v. 223, no. 1-2, p. 17-34.

Ruscitto, D. M., Wallace, P. J., Cooper, L. B., and Plank, T., 2012, Global variations in H2O/Ce: 2. Relationships to arc magma geochemistry and volatile fluxes: Geochemistry Geophysics Geosystems, v. 13, no. 3, p. Q03025, DOI: 03010.01029/02011gc003887.

Saal, A. E., Hauri, E. H., Langmuir, C. H., and Perfit, M. R., 2002, Vapour undersaturation in primitive mid-ocean-ridge basalt and the volatile content of Earth's upper mantle: Nature, v. 419, no. 6906, p. 451-455.

Sadofsky, S. J., and Bebout, G. E., 2003, Record of forearc devolatilization in low-T, high-P/T metasedimentary suites: Significance for models of convergent margin chemical cycling: Geochemistry, Geophysics, Geosystems, v. 4, no. 4, p. 9003, doi:9010.1029/2002GC000412.

Savov, I. P., Ryan, J. G., D'Antonio, M., and Fryer, P., 2007, Shallow slab fluid release across and along the Mariana arc-basin system: Insights from geochemistry of serpentinized peridotites from the Mariana fore arc: Journal of Geophysical Research, v. 112, no. B9, p. B09205, DOI: 09210.01029/02006JB004749.

860 Scambelluri, M., Bottazzi, P., Trommsdorff, V., Vannucci, R., Hermann, J., Gòmez-Pugnaire,
861 M. T., and Lòpez-Sànchez Vizcaìno, V., 2001, Incompatible element-rich fluids
862 released by antigorite breakdown in deeply subducted mantle: Earth and Planetary
863 Science Letters, v. 192, no. 3, p. 457-470.
864 Schiano, P., 2003, Primitive mantle magmas recorded as silicate melt inclusions in igneous
865 minerals: Earth-Science Reviews, v. 63, no. 1–2, p. 121-144.
866 Schmidt, M., and Poli, S., 1998, Experimentally based water budgets for dehydrating slabs
867 and consequences for magma generation: Earth and Planetary Science Letters, v.
868 163, no. 1-4, p. 361-379.
869 Shervais, J. W., Reagan, M., Haugen, E., Almeev, R. R., Pearce, J. A., Prytulak, J., Ryan, J. G.,
870 Whattam, S. A., Godard, M., Chapman, T., Li, H., Kurz, W., Nelson, W. R., Heaton, D.
871 E., Kirchenbaur, M., Shimizu, K., Sakuyama, T., Li, Y., and Vetter, S. K., 2019,
872 Magmatic Response to Subduction Initiation: Part 1. Fore-arc Basalts of the Izu-Bonin
873 Arc From IODP Expedition 352: Geochemistry Geophysics Geosystems, v. 20, no. 1, p.
874 314-338.
875 Shervais, J. W., Reagan, M. K., Godard, M., Prytulak, J., Ryan, J. G., Pearce, J. A., Almeev, R.
876 R., Li, H., Haugen, E., Chapman, T., Kurz, W., Nelson, W. R., Heaton, D. E.,
877 Kirchenbaur, M., Shimizu, K., Sakuyama, T., Vetter, S. K., Li, Y., and Whattam, S. A.,
878 2021, Magmatic Response to Subduction Initiation, Part II: Boninites and Related
879 Rocks of the Izu-Bonin Arc From IOPD Expedition 352: Geochemistry Geophysics
880 Geosystems, v. 22, no. 1, p. e2020GC009093,
881 https://doi.org/009010.001029/002020GC009093.
882 Stern, R. J., and Bloomer, S. H., 1992, Subduction zone infancy: Examples from the Eocene
883 Izu-Bonin-Mariana and Jurassic California arcs: Geological Society of America
884 Bulletin, v. 104, no. 12, p. 1621-1636.
885 Stern, R. J., Fouch, M., and Klemperer, S. L., 2003, An Overview of the Izu-Bonin-Mariana
886 Subduction Factory, *in* Eiler, J., and Hirschmann, M., eds., Inside the subduction
887 factory, Volume 138: Washington, D.C., Geophysical Monograph Series, p. 175-222.
888 Stern, R. J., Tamura, Y., Ishizuka, O., Shukano, H., Bloomer, S. H., Embley, R. W., Leybourne,
889 M., Kawabata, H., Nunokawa, A., Nichols, A. R. L., Kohut, E., and Pujana, I., 2013a,
890 Volcanoes of the Diamante cross-chain: evidence for a mid-crustal felsic magma
891 body beneath the Southern Izu–Bonin–Mariana arc: Geological Society, London,
892 Special Publications, v. 385, https://doi.org/10.1144/SP385.6.
893 Stern, R. J., Tamura, Y., Masuda, H., Fryer, P., Martinez, F., Ishizuka, O., and Bloomer, S. H.,
894 2013b, How the Mariana Volcanic Arc ends in the south: Island Arc, v. 22, p. 133-148.
895 Straub, S. M., Goldstein, S. L., Class, C., Schmidt, A., and Gomez-Tuena, A., 2010, Slab and
896 Mantle Controls on the Sr–Nd–Pb–Hf Isotope Evolution of the Post 42 Ma Izu–Bonin
897 Volcanic Arc: Journal of Petrology, v. 51, no. 5, p. 993-1026.
898 Straub, S. M., Woodhead, J. D., and Arculus, R. J., 2015, Temporal Evolution of the Mariana
899 Arc: Mantle Wedge and Subducted Slab Controls Revealed with a Tephra
900 Perspective: Journal of Petrology, v. 56, no. 2, p. 409-439.
901 Tamura, Y., Ishizuka, O., Stern, R. J., Nichols, A. R. L., Kawabata, H., Hirahara, Y., Chang, Q.,
902 Miyazaki, T., Kimura, J., Embley, R. W., and Tatsumi, Y., 2014, Mission Immiscible:
903 Distinct Subduction Components Generate Two Primary Magmas at Pagan Volcano,
904 Mariana Arc: Journal of Petrology, v. 55, no. 1, p. 63-101.
905 Tamura, Y., Ishizuka, O., Stern, R. J., Shukuno, H., Kawabata, H., Embley, R. W., Hirahara, Y.,
906 Chang, Q., Kimura, J.-I., Tatsumi, Y., Nunokawa, A., and Bloomer, S. H., 2011, Two

Primary Basalt Magma Types from Northwest Rota-1 Volcano, Mariana Arc and its Mantle Diapir or Mantle Wedge Plume: Jounal of Petrology, v. 52, no. 6, p. 1143-1183.

Figure captions

Fig. 1: Subduction inception vs. modern near-trench spreading. A) Sketch of near-trench spreading that occurred during subduction inception, such as in the Eocene IBM proto-arc crust. B) Sketch of the Southern Mariana fore-arc rifts (SEMFR), which represents a modern near-trench spreading center that developed in the fore-arc above a mature subduction zone in Pliocene time. The Southern Mariana is characterized by the occurrence of infant arc volcanoes (the Fina-Nagu volcanic chain) and a back-arc basin (BAB) spreading center, the Malaguana-Gadao Ridge (MGR). Although the SEMFR share some similarities with the IBM proto-arc crusts, these geological features are not observed during subduction inception; and they are instead typical of long-lived subduction zones.

Fig. 2: Bathymetric map of the Izu-Bonin-Mariana convergent margin (http://www.geomapapp.org). The map shows the location of the IODP Site 352 (Reagan et al., 2017), Bonin Island (Ishizuka et al., 2020; Kanayama et al., 2012, 2014), southern Mariana fore-arc rifts (SEMFR) (Ribeiro et al., 2013a; Ribeiro et al., 2013b), and of the Eocene proto-arc crust from the southern Marianas (Reagan et al., 2010).

Fig. 3: **Composition of the magmas**. A) SiO_2 vs. K_2O diagram used to classify rocks (Peccerillo and Taylor, 1976). B) MgO vs. TiO_2 diagram. The southern Mariana olivine-hosted melt inclusions are primitive basalts with a boninitic fingerprint. The boninitic compositional field is from Pearce and Reagan (2019). C-D) MgO vs. SiO_2 classification diagram of Pearce and Reagan (2019) used to distinguish low- and high-Si boninites. We compiled glass shards and olivine-hosted melt inclusions for the IBM proto-arc magmas and for the SEMFR magmas to ensure freshness, and bulk rocks for the IBM infant arc as there were no available data for basaltic glass shards. White numbers in black circles (from 1 to 5) refers to the compositional evolution of the magma over time. These numbers also refer to the sequence of event the caption, as well as to the sequence of events outlined in the discussion.

Fig. 4: Composition of the slab fluids released during subduction inception. A) Th/Nb vs. Nb/Yb and B) Ba/Th vs. Rb/Th diagrams, after Pearce et al. (2005), showing enrichments in sediment melts (Th/Nb) and in water-rich, slab fluids (Ba/Th, Rb/Th) in the magmas. The IBM boninites and the SEMFR basalts and associated olivine-hosted melt inclusions display high slab fluid markers in Rb/Th and Ba/Th, indicating that they captured water-rich slab fluids. The light green, dark green and blue rectangles represent the fluid composition (water-rich fluid and solute-rich fluid) released from the subducted sediments (sed.), the subducted serpentinites, and the altered oceanic crust (AOC), respectively. The composition of the slab fluids were assessed using the bulk sediment composition of the Mariana composite, Site 800 (Plank and Langmuir, 1998) and the partition coefficients for melting and dehydration of the subducted sediments (Johnson and Plank, 1999), the composition of the crust composite of Site 801 ("SUPER") (Kelley et al., 2003) and the partition coefficients for dehydrating the oceanic crust (Kessel et al., 2005), and the composition of olivine-hosted fluid inclusions from serpentinized mantle rocks (Ribeiro et al., 2015). See text and Table S2 for details.

Fig. 5: Composition of the water-rich slab fluids released during subduction inception. A) H_2O/Ce, B) Cs/Th and C) Cs/Ba vs Rb/Th diagrams showing the strong enrichment in water-rich slab fluids of the SEMFR basalts and proto-arc boninites glasses from IBM, as compared to the IBM arc and back-arc basalts. The light green, dark green and blue rectangles represent the slab fluid composition released from the subducted sediments (sed.), the subducted serpentinites, and the altered oceanic crust (AOC), respectively. See Fig. 3 for details about the slab fluid composition.

Fig. 6: Melting of the oceanic crust in the amphibolite facies during subduction inception. A) Zr/Sm and B) Hf/Sm vs. La/Sm diagrams of Pearce et al. (1992) showing that melts from the oceanic crust infiltrated the depleted mantle source of the low-silica and high-silica boninites in IBM.

Fig. 7: Variations of the water-rich slab fluids with the distance to the trench in IBM. A) H_2O/Ce and B) Rb/Th vs. trench distance. The highest H_2O/Ce and Rb/Th ratios in the IBM boninites suggest that there is a peak in slab dehydration in IBM within 1-2 Myr after the onset of subduction, which rapidly decreases with time and trench distance, as the arc develops. Similar ratios are also observed in the SEMFR magmas, indicating that a peak in slab dehydration may also occur within 90 km from the trench in long-lived, cold subduction zones (Johnson and Plank, 1999). We used the estimated distance to the trench for the IBM FABs (~20- 30 km) and IBM boninites (~40 - 60 km) of Reagan et al. (2019). The trench distance for the infant arc (~80 ± 25 km) was assessed from the current location of Hahajima (Ishizuka et al., 2020), which represent preserved infant arc volcanoes that formed in Eocene time. A trench distance of 200 ± 25 km was estimated for the Mariana arc, and of 300 ± 25 km for the Mariana Trough. Trench distance for the SEMFR glasses (± 5 km) is from Ribeiro et al. (2013a).

Fig. 8: Sources of the slab fluids throughout the lifetime of IBM. A) Ba/Th vs. $^{206}Pb/^{204}Pb$ and B) Ba/Th vs. $^{87}Sr/^{86}Sr$ diagrams show that the subducted mantle and the altered oceanic crust dehydrate first to contribute to fingerprint the IBM boninites. The composition of the subducted sediments in $^{206}Pb/^{204}Pb$ cannot explain the compositional variations observed in the magmas (panel A). C) Th/Nb vs. $^{206}Pb/^{204}Pb$ and D) vs. $^{207}Pb/^{206}Pb$ diagrams showing the enrichment in sediment melts into the mature arc magmas. D) We used bulk rock composition for all samples as radiogenic isotopes were not measured on glass shards. Because Ba, Th and Nb are less sensitive to secondary alteration processes than Cs and Rb, Ba/Th, and Th/Nb were used to track the slab fluid contribution. Details about the end-members and the mixing equations are provided in the supplementary material and in Table S2. AOC: altered oceanic crust, sed: sediments, serp: serpentinized mantle. The black start represents the estimated mantle composition of Ribeiro et al. (2013b).

Fig. 9: Sources of the slab fluids in the SEMFR magmas. A) Ba/Th vs. $^{206}Pb/^{204}Pb$ and B) vs. $^{87}Sr/^{86}Sr$ diagrams showing the contribution of the altered oceanic crust (AOC) and serpentinized mantle (serp) in the water-rich fluids released beneath the southern Mariana fore-arc. C) Th/Nb vs. $^{206}Pb/^{204}Pb$ and D) vs. $^{207}Pb/^{206}Pb$ diagrams showing the reduced enrichment in sediment melts into the SEMFR magmas. The composition of the SEMFR magmas overlap that of the LSB. We plotted the bulk composition of the magmas as isotopic composition were only measured in whole rocks. For this reason, we selected Ba and Th to track the slab fluids as in Pearce et al. (2005), as these elements are less prone to alteration than Cs and Rb.

Fig. 10: Pb isotopic composition of the IBM and SEMFR magmas. A-B) $^{206}Pb/^{204}Pb$ vs. $^{208}Pb/^{206}Pb$ and C-D) $^{206}Pb/^{204}Pb$ vs. $^{207}Pb/^{206}Pb$ diagrams showing the various contribution in sediments and altered oceanic crust in the SEMFR (B, D) and IBM magmas over time (A, C). The white numbers in a black circle represent the time sequence of the IBM magmas (see figure caption for details).

Fig. 11: Sketch illustrating slab dehydration and melting following subduction inception. A) During subduction inception, FABs form by decompression melting within a few kilometers from the trench. Large fluxes of water-rich fluids are rapidly released within 90 km from the trench from dehydrating the subducted mantle and the altered oceanic crust (AOC) within 2 – 3 Myr following subduction inception. The nascent, warm slab also melts in the amphibolite facies. B) In IBM, the increasing fluxing of the highly depleted mantle source produces the HSB. The HSB marks the transition from adiabatic decompression to fluid-assisted mantle melting. Eruption of the HSB terminates shortly after the development of the infant volcanic arc within 5 to 10 Ma following subduction inception. The slab capacity to carry volatiles diminishes with increasing slab depth, so that the infant arc magmas capture less water-rich slab fluids, as they are migrating away from the trench. C) As the volcanic arc front reach maturation, the IBM volcanic arc front is at ~200 km from the trench and capture slab fluids released from a deeper part of the slab. The deeper slab fluids are less enriched in water (Rb, Cs) and more enriched in total dissolved solutes and K. The contribution of the sediment melts into the arc magmas thus increases with time and increasing slab depth. This evolution and subsequent stabilization of the subduction zone is permitted by slab dehydration at shallow depth, that is associated serpentinization of the fore-arc mantle since arc inception.

Supplementary material

Table S1: Compiled dataset for major and trace element composition of the fresh glass shards and olivine-hosted melt inclusions from the Southern Marianas, the Mariana arc and back-arc basin, and the Izu-Bonin-Mariana proto-arc crust.

Table S2: Composition of the end-members and slab fluid composition used for the mixing equations.

A- Subduction inception

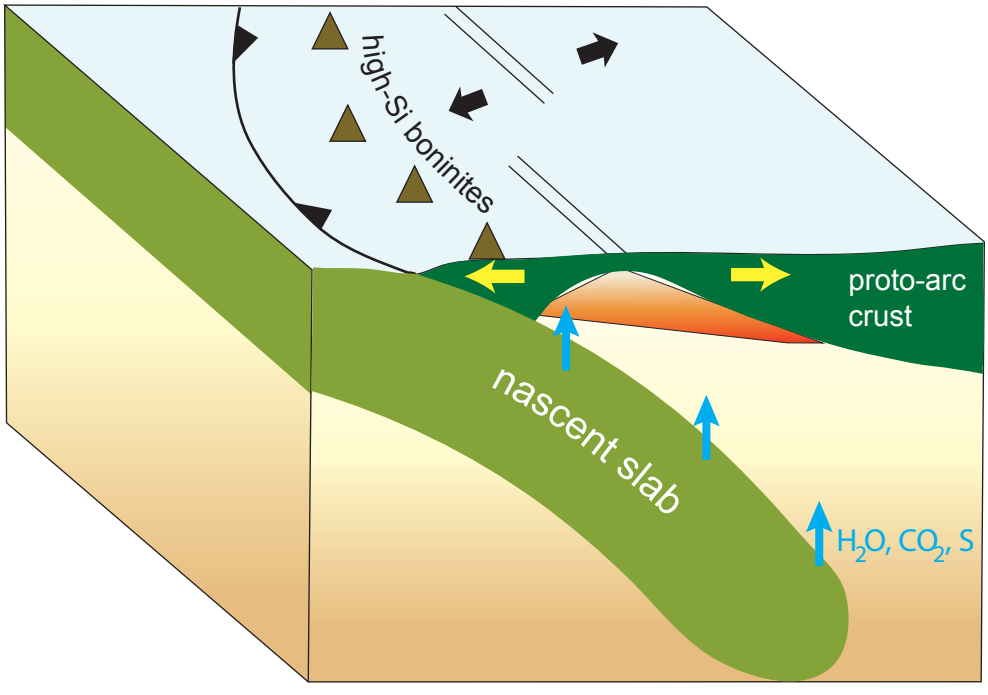

B- SEMFR: modern near-trench spreading

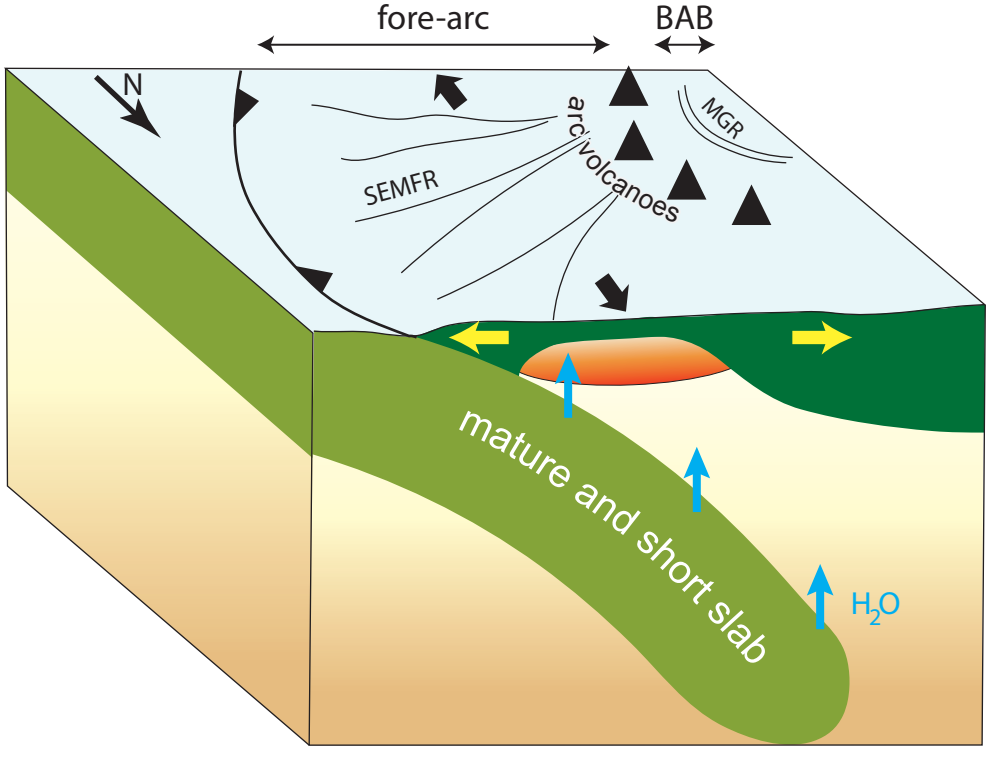

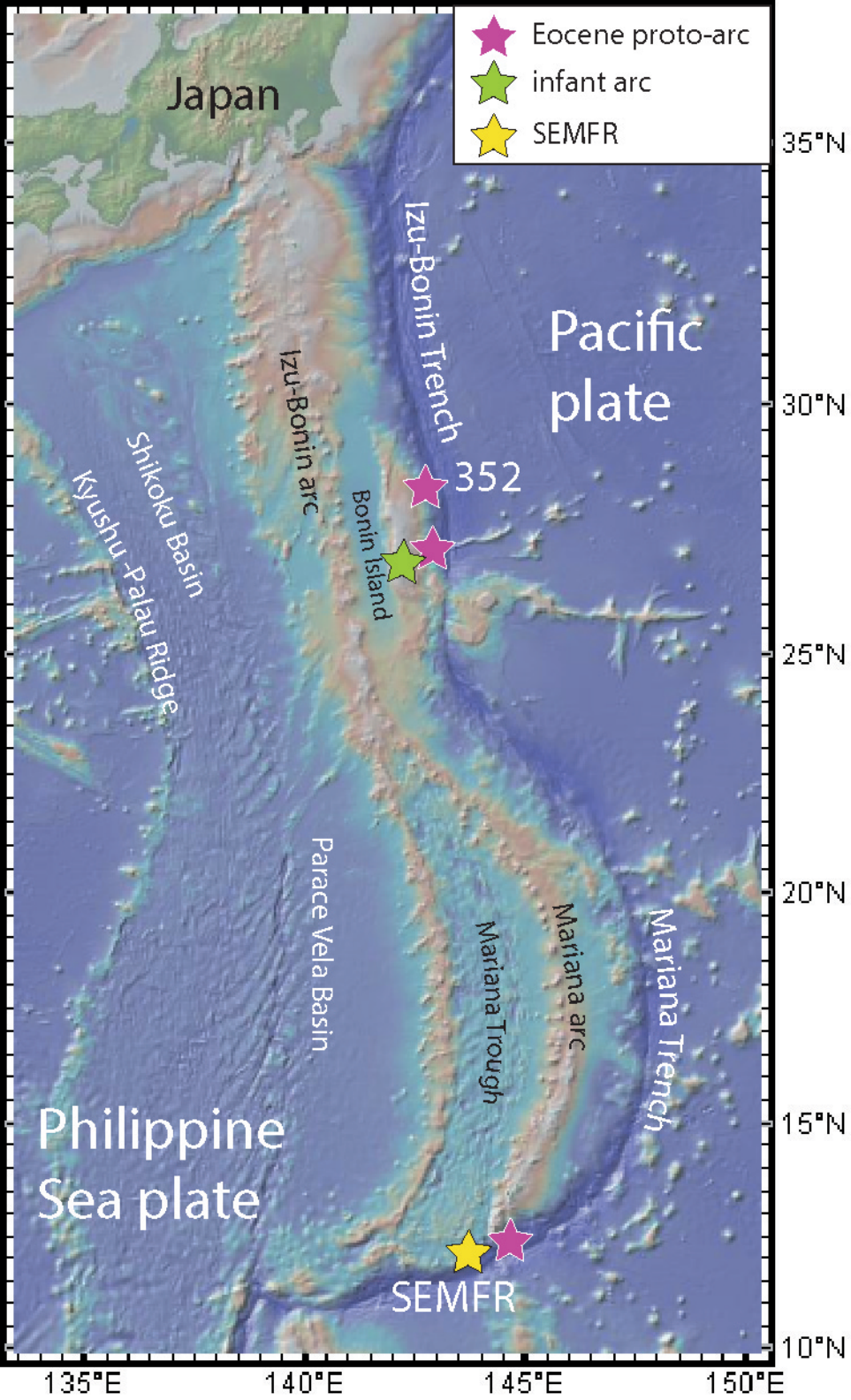
Eocene proto-arc
infant arc
SEMFR
Japan
Izu-Bonin Trench
Pacific plate
Izu-Bonin arc
Shikoku Basin
Kyushu -Palau Ridge
352
Bonin Island
Parace Vela Basin
Mariana Trough
Mariana arc
Mariana Trench
Philippine Sea plate
SEMFR
35°N
30°N
25°N
20°N
15°N
10°N
135°E
140°E
145°E
150°E

Fig. 2

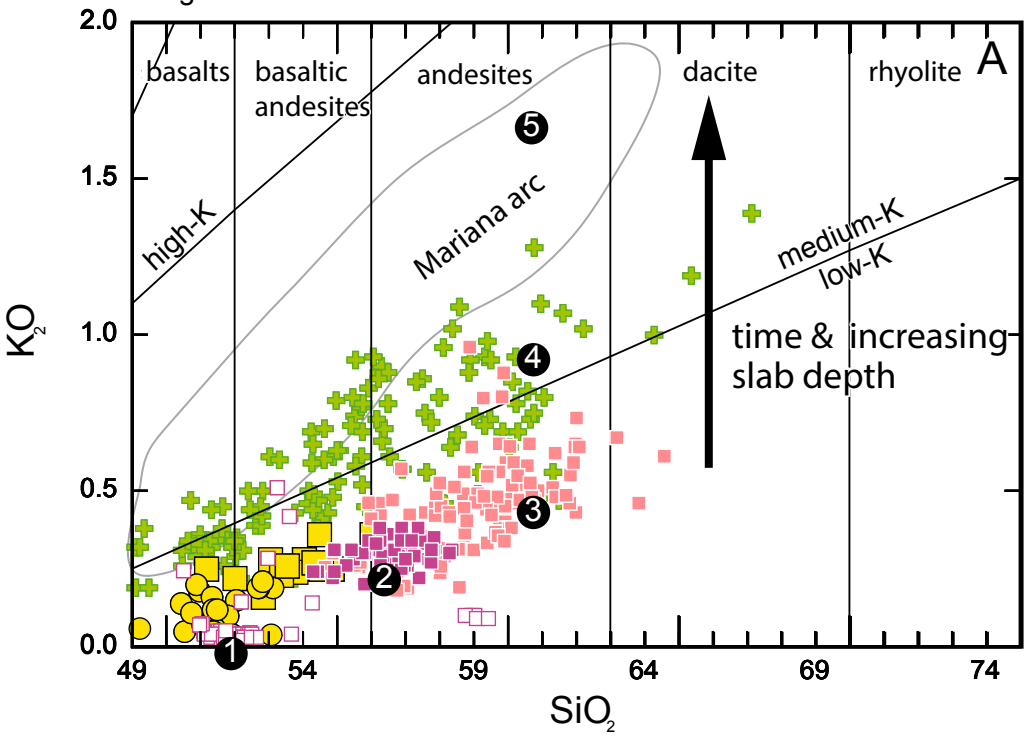
A
basalts
basaltic andesites
andesites
dacite
rhyolite
high-K
medium-K
low-K
Mariana arc
time & increasing slab depth
1
2
3
4
5
K2O
SiO2
0.0
0.5
1.0
1.5
2.0
49
54
59
64
69
74

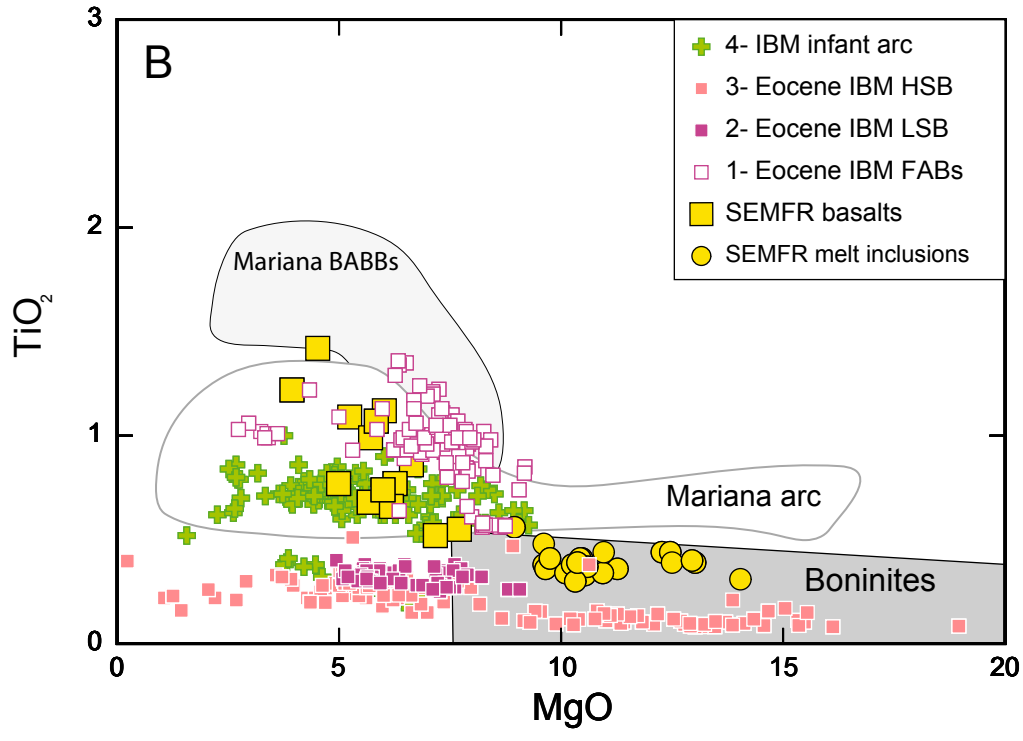
B
4- IBM infant arc
3- Eocene IBM HSB
2- Eocene IBM LSB
1- Eocene IBM FABs
SEMFR basalts
SEMFR melt inclusions
Mariana BABBs
Mariana arc
Boninites
TiO2
MgO
0
1
2
3
0
5
10
15
20

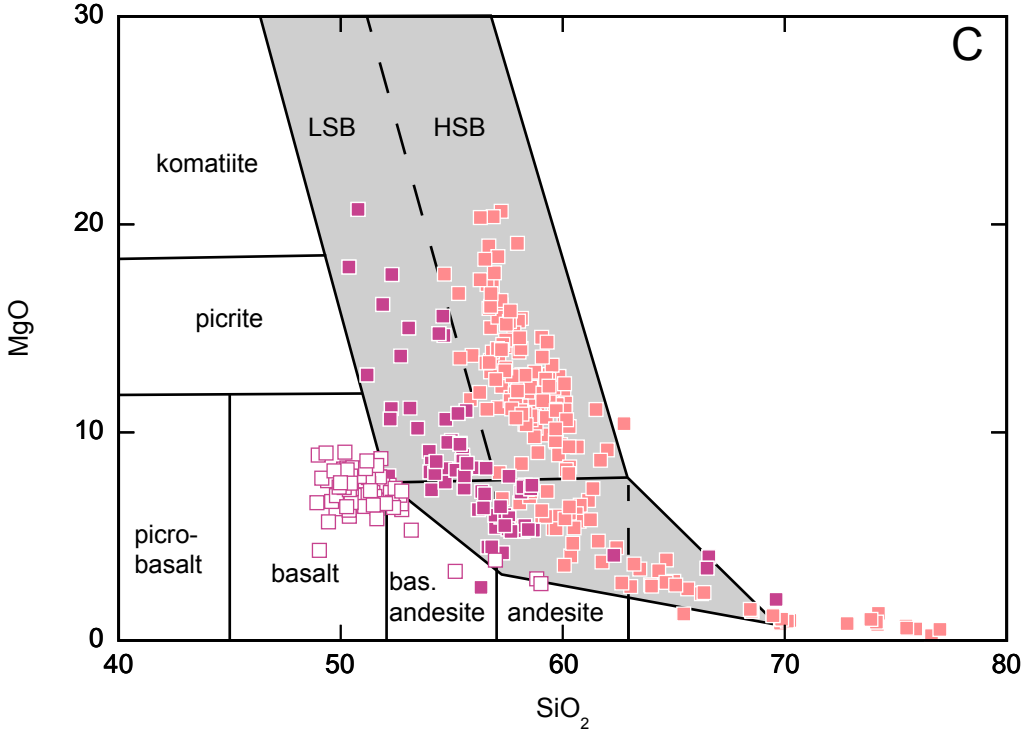
C
LSB
HSB
komatiite
picrite
picro-basalt
basalt
bas. andesite
andesite
MgO
SiO2
0
10
20
30
40
50
60
70
80

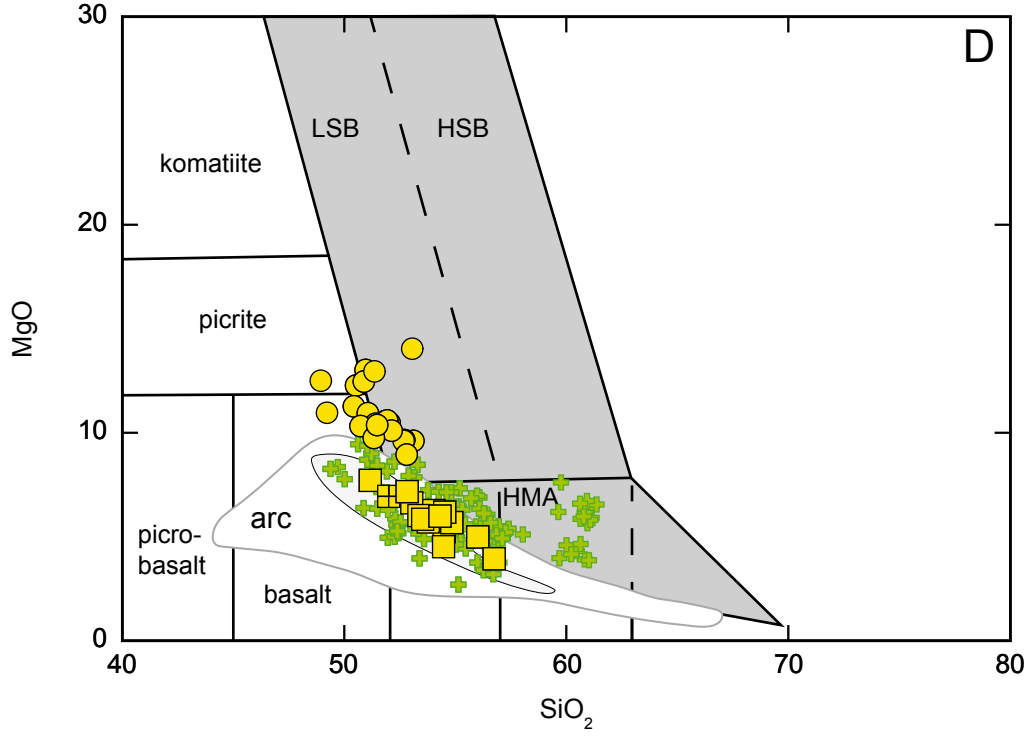
D
LSB
HSB
komatiite
picrite
picro-basalt
basalt
arc
HMA
MgO
SiO2
0
10
20
30
40
50
60
70
80

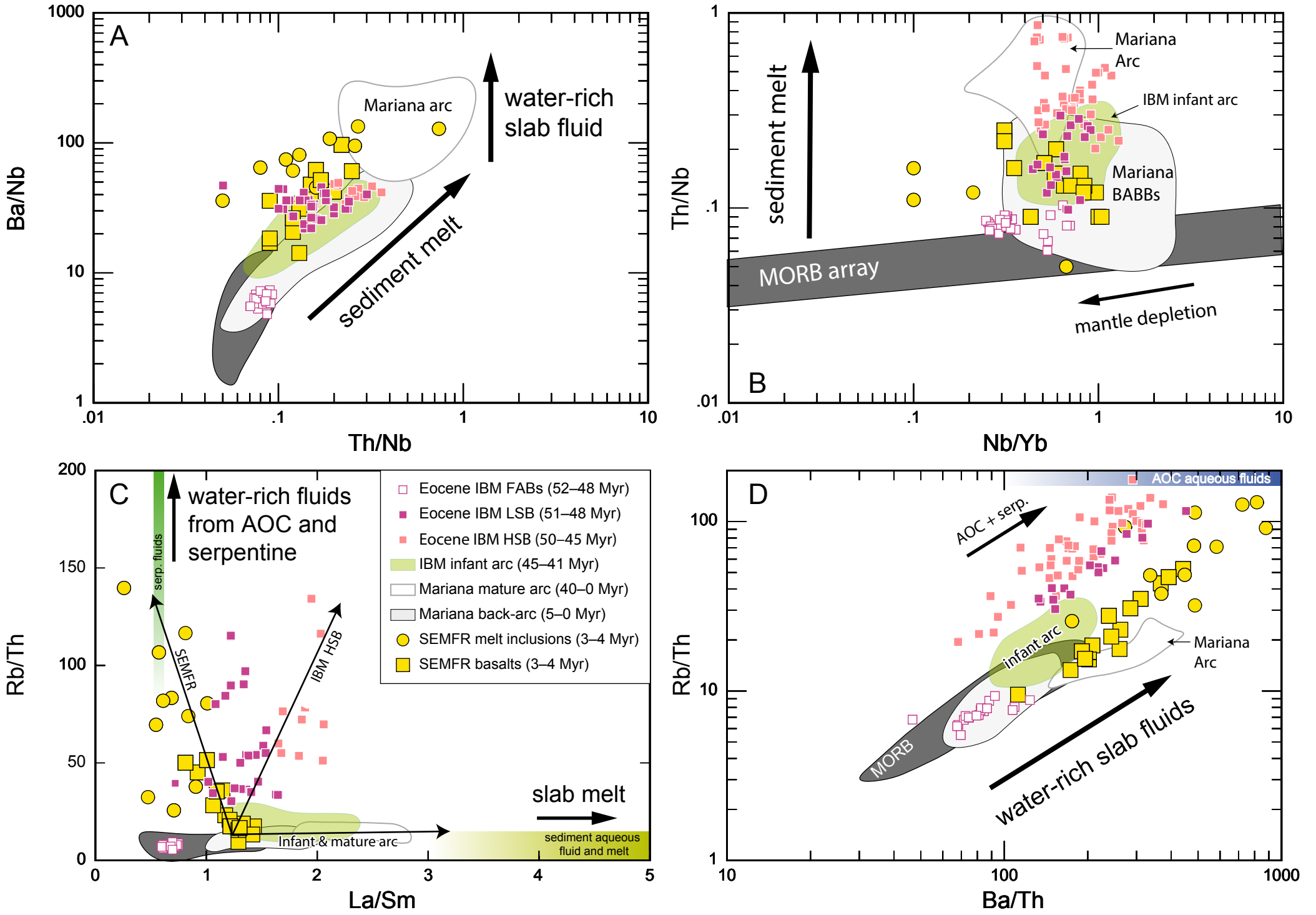
A
Ba/Nb
Th/Nb
Mariana arc
water-rich
slab fluid
sediment melt
B
Th/Nb
Nb/Yb
sediment melt
Mariana
Arc
IBM infant arc
Mariana
BABBs
MORB array
mantle depletion
C
Rb/Th
La/Sm
water-rich fluids
from AOC and
serpentine
serp. fluids
SEMFR
IBM HSB
Eocene IBM FABs (52–48 Myr)
Eocene IBM LSB (51–48 Myr)
Eocene IBM HSB (50–45 Myr)
IBM infant arc (45–41 Myr)
Mariana mature arc (40–0 Myr)
Mariana back-arc (5–0 Myr)
SEMFR melt inclusions (3–4 Myr)
SEMFR basalts (3–4 Myr)
slab melt
Infant & mature arc
sediment aqueous
fluid and melt
D
Rb/Th
Ba/Th
AOC aqueous fluids
AOC + serp.
infant arc
Mariana
Arc
MORB
water-rich slab fluids

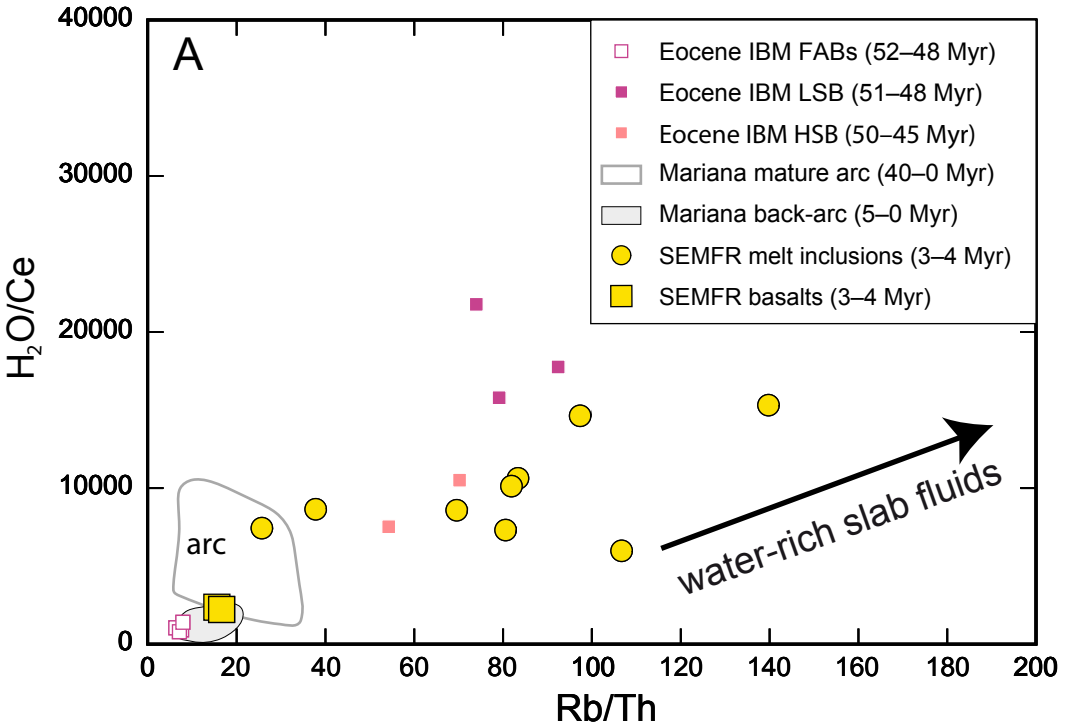
A
Eocene IBM FABs (52–48 Myr)
Eocene IBM LSB (51–48 Myr)
Eocene IBM HSB (50–45 Myr)
Mariana mature arc (40–0 Myr)
Mariana back-arc (5–0 Myr)
SEMFR melt inclusions (3–4 Myr)
SEMFR basalts (3–4 Myr)
arc
water-rich slab fluids
H2O/Ce
Rb/Th
40000
30000
20000
10000
0
0
20
40
60
80
100
120
140
160
180
200

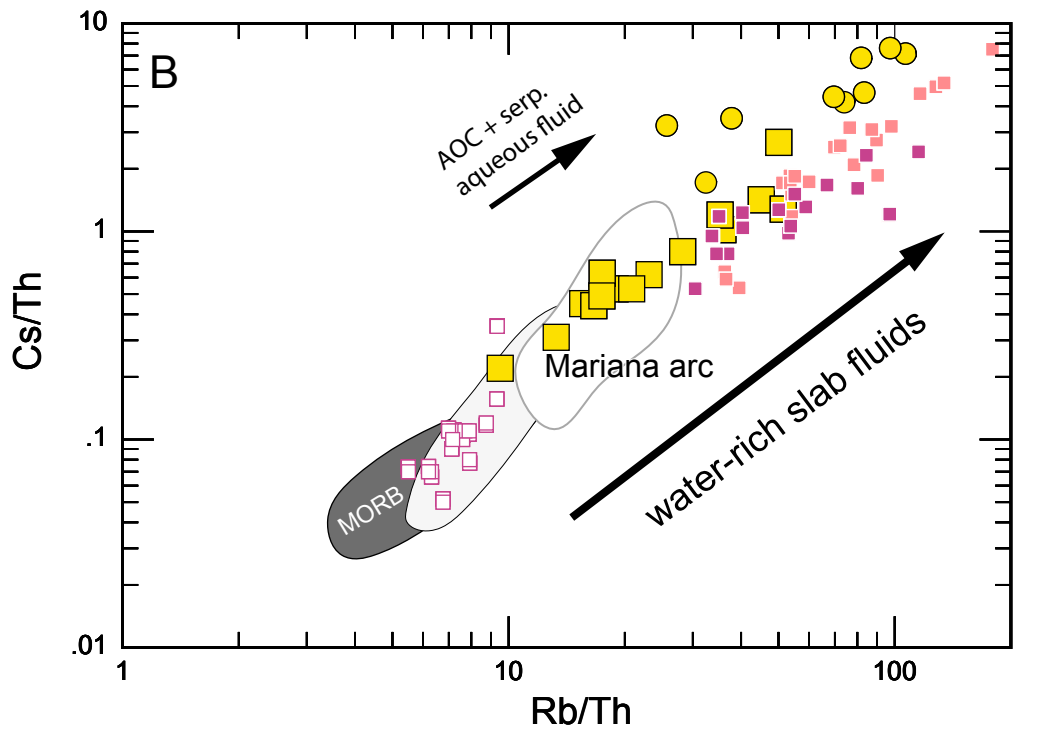
B
AOC + serp. aqueous fluid
Mariana arc
MORB
water-rich slab fluids
Cs/Th
Rb/Th
10
1
.1
.01
1
10
100

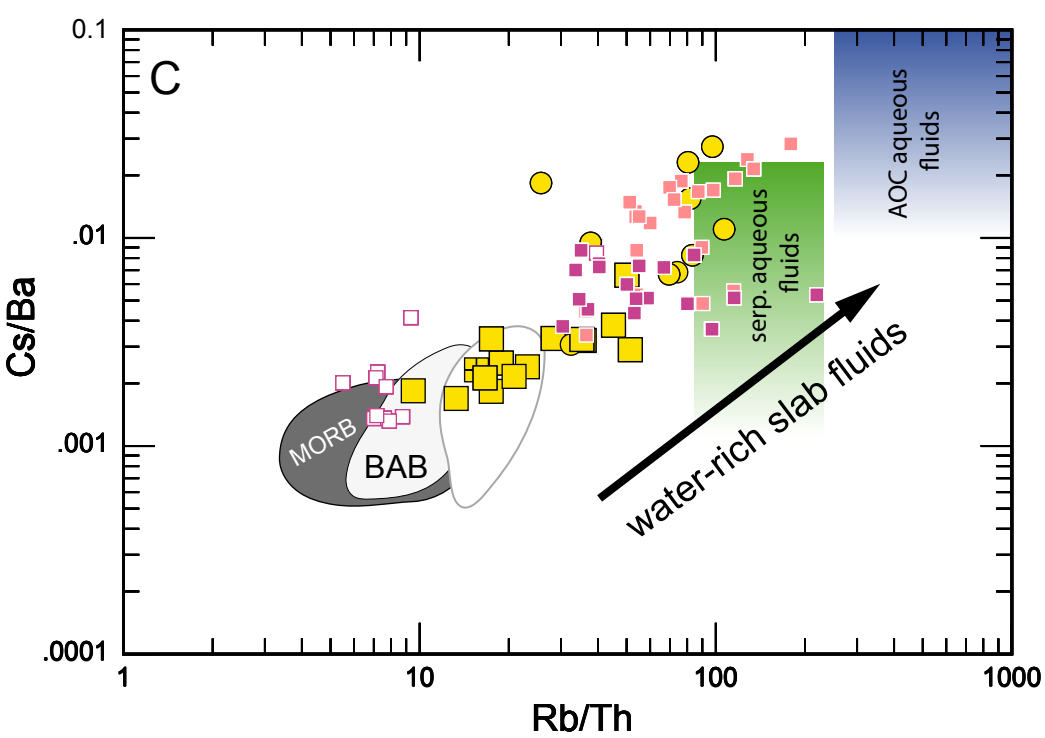
C
AOC aqueous fluids
serp. aqueous fluids
MORB
BAB
water-rich slab fluids
Cs/Ba
Rb/Th
0.1
.01
.001
.0001
1
10
100
1000

Fig. 6

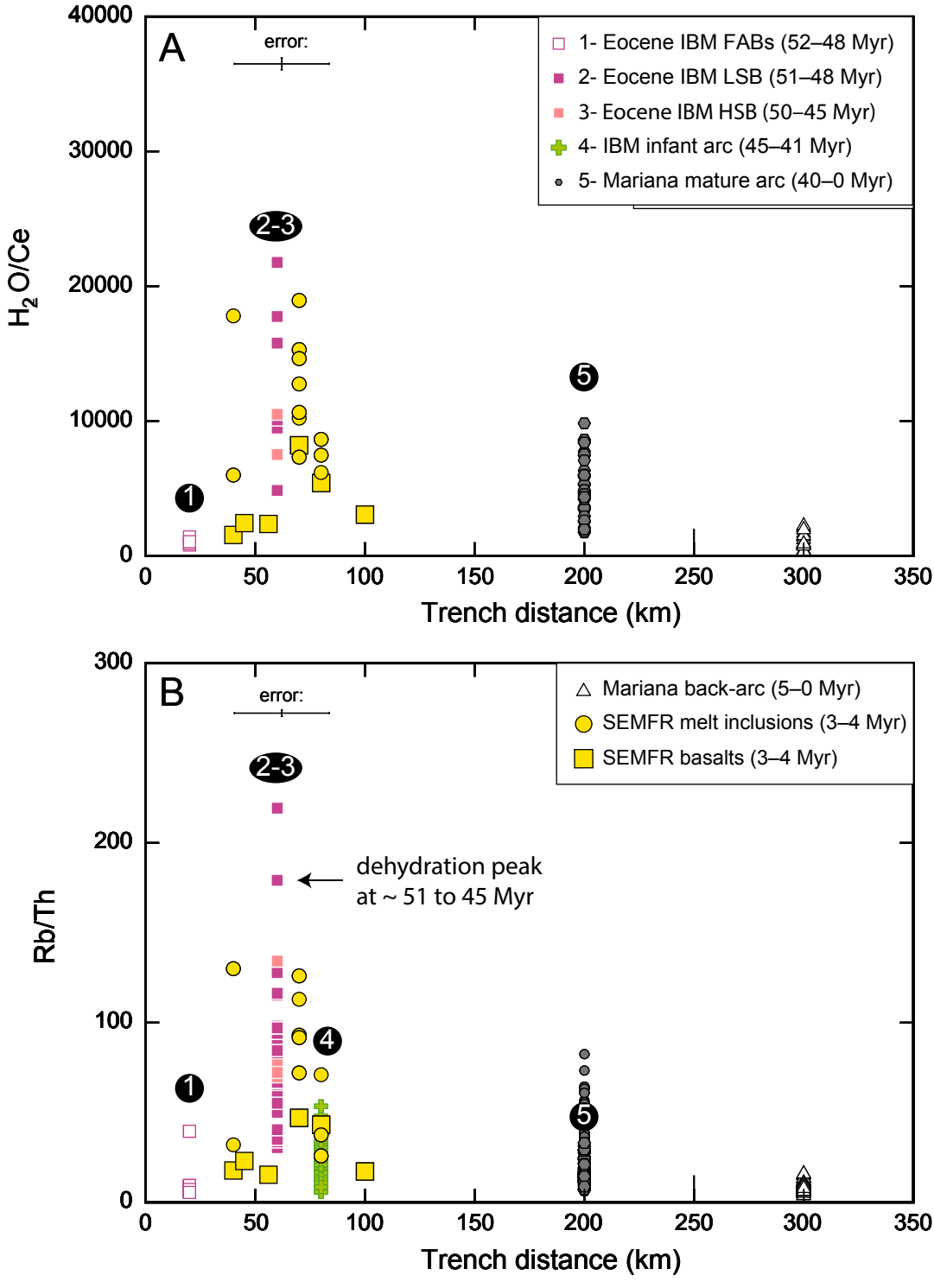
A
error:
1- Eocene IBM FABs (52–48 Myr)
2- Eocene IBM LSB (51–48 Myr)
3- Eocene IBM HSB (50–45 Myr)
4- IBM infant arc (45–41 Myr)
5- Mariana mature arc (40–0 Myr)
H2O/Ce
Trench distance (km)
B
error:
Mariana back-arc (5–0 Myr)
SEMFR melt inclusions (3–4 Myr)
SEMFR basalts (3–4 Myr)
dehydration peak
at ~ 51 to 45 Myr
Rb/Th
Trench distance (km)

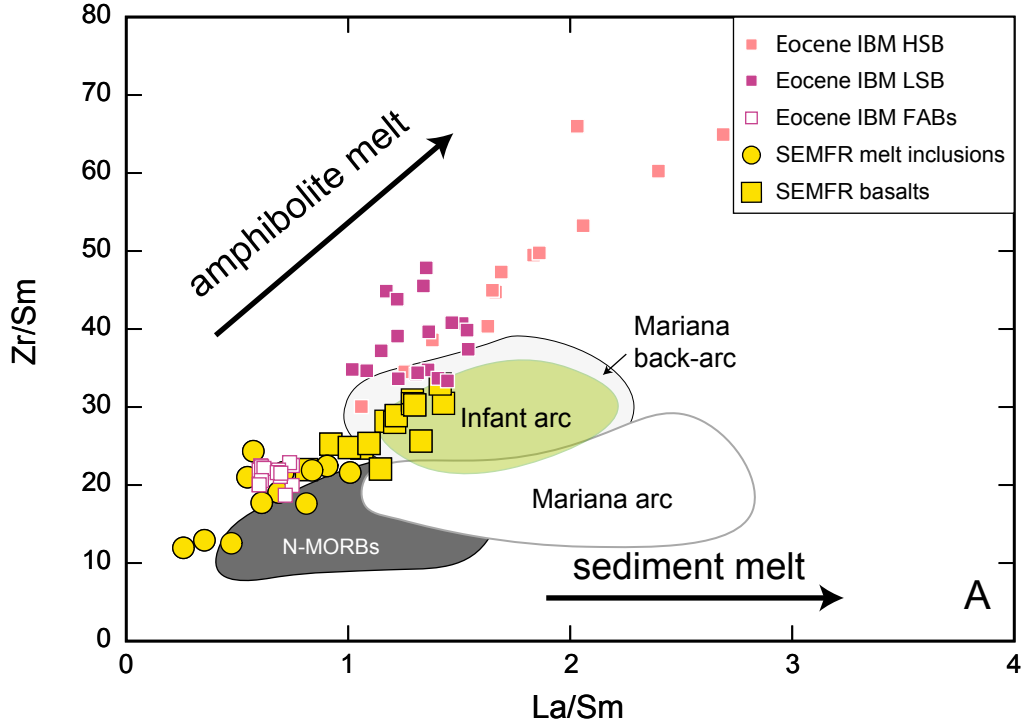
Eocene IBM HSB
Eocene IBM LSB
Eocene IBM FABs
SEMFR melt inclusions
SEMFR basalts
amphibolite melt
Mariana
back-arc
Infant arc
Mariana arc
N-MORBs
sediment melt
A
Zr/Sm
La/Sm
0
10
20
30
40
50
60
70
80
1
2
3
4

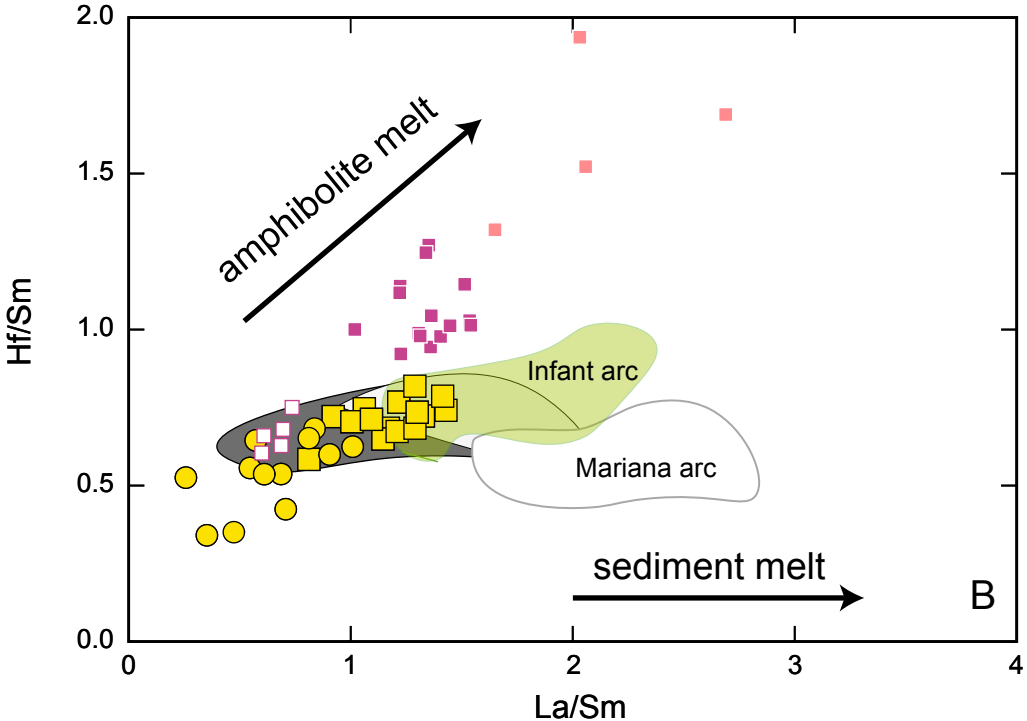
amphibolite melt
Infant arc
Mariana arc
sediment melt
B
Hf/Sm
La/Sm
0.0
0.5
1.0
1.5
2.0
1
2
3
4

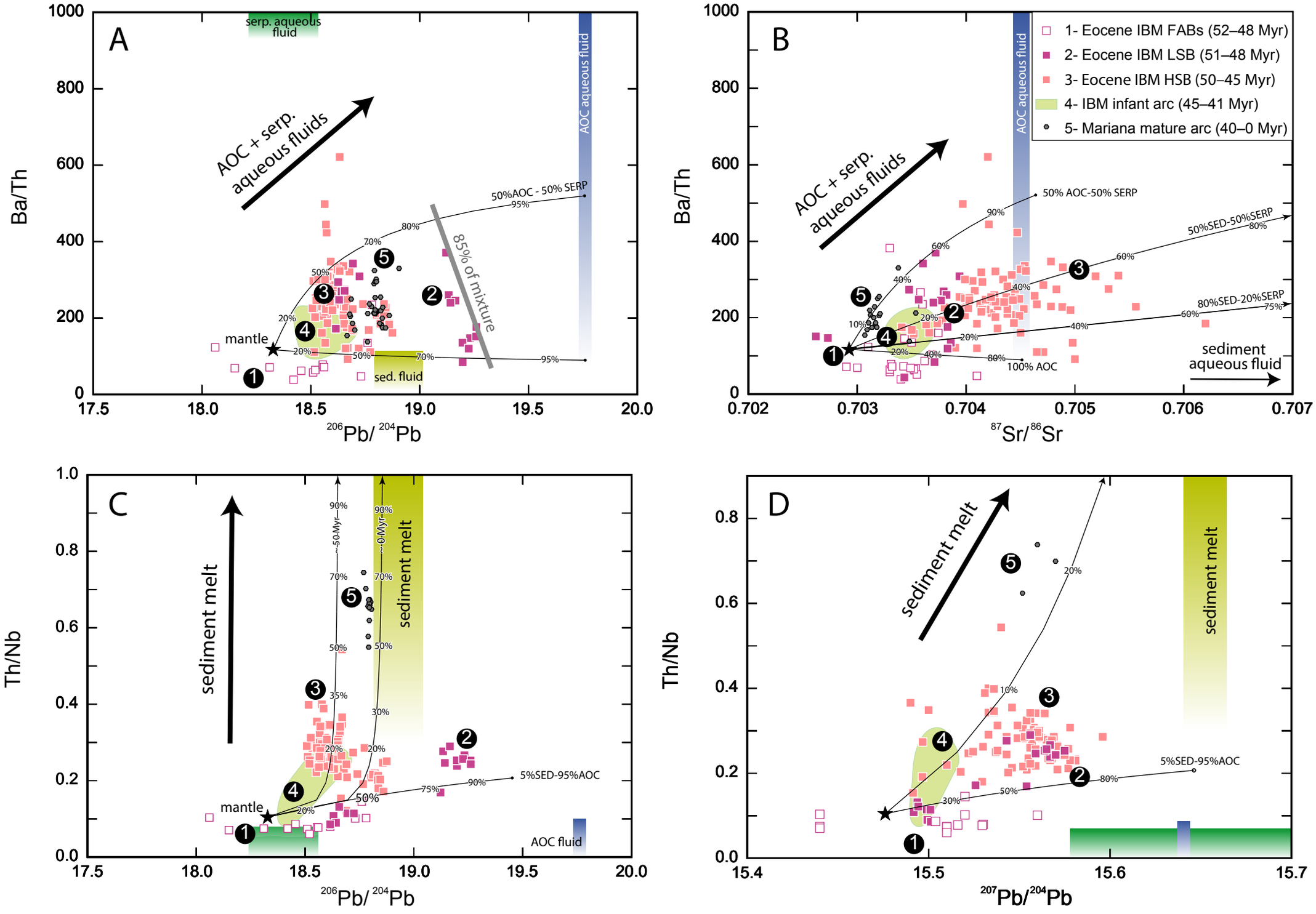
A
serp. aqueous fluid
AOC aqueous fluid
AOC + serp. aqueous fluids
50%AOC - 50% SERP
95%
80%
70%
50%
20%
85% of mixture
mantle
sed. fluid
Ba/Th
206Pb/ 204Pb
B
1- Eocene IBM FABs (52–48 Myr)
2- Eocene IBM LSB (51–48 Myr)
3- Eocene IBM HSB (50–45 Myr)
4- IBM infant arc (45–41 Myr)
5- Mariana mature arc (40–0 Myr)
AOC aqueous fluid
AOC + serp. aqueous fluids
50% AOC-50% SERP
50%SED-50%SERP
80%SED-20%SERP
100% AOC
sediment aqueous fluid
Ba/Th
87Sr/86Sr
C
sediment melt
~50 Myr
~0 Myr
sediment melt
5%SED-95%AOC
mantle
AOC fluid
Th/Nb
206Pb/ 204Pb
D
sediment melt
sediment melt
5%SED-95%AOC
Th/Nb
207Pb/204Pb

Fig. 8

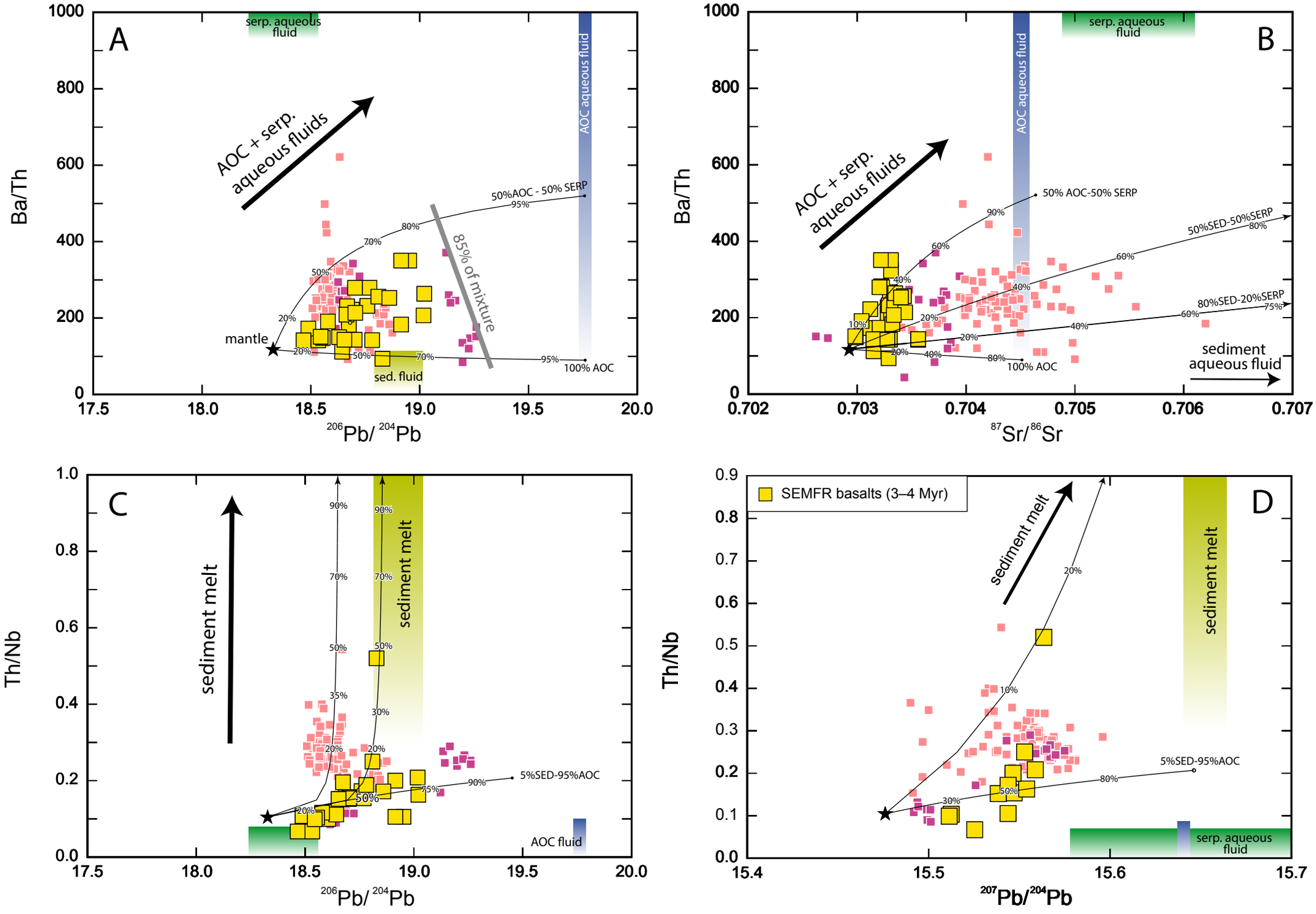
A
serp. aqueous fluid
AOC aqueous fluid
AOC + serp. aqueous fluids
50%AOC - 50% SERP
95%
80%
70%
50%
20%
85% of mixture
mantle
20%
50%
70%
95%
100% AOC
sed. fluid
Ba/Th
206Pb/ 204Pb
B
serp. aqueous fluid
AOC aqueous fluid
AOC + serp. aqueous fluids
50% AOC-50% SERP
90%
60%
40%
20%
10%
50%SED-50%SERP
80%
60%
40%
20%
80%SED-20%SERP
75%
60%
40%
20%
80%
100% AOC
sediment aqueous fluid
Ba/Th
87Sr/86Sr
C
sediment melt
sediment melt
90%
70%
50%
35%
30%
20%
20%
5%SED-95%AOC
90%
75%
50%
20%
AOC fluid
Th/Nb
206Pb/ 204Pb
D
SEMFR basalts (3–4 Myr)
sediment melt
sediment melt
20%
10%
5%SED-95%AOC
80%
50%
30%
serp. aqueous fluid
Th/Nb
207Pb/204Pb

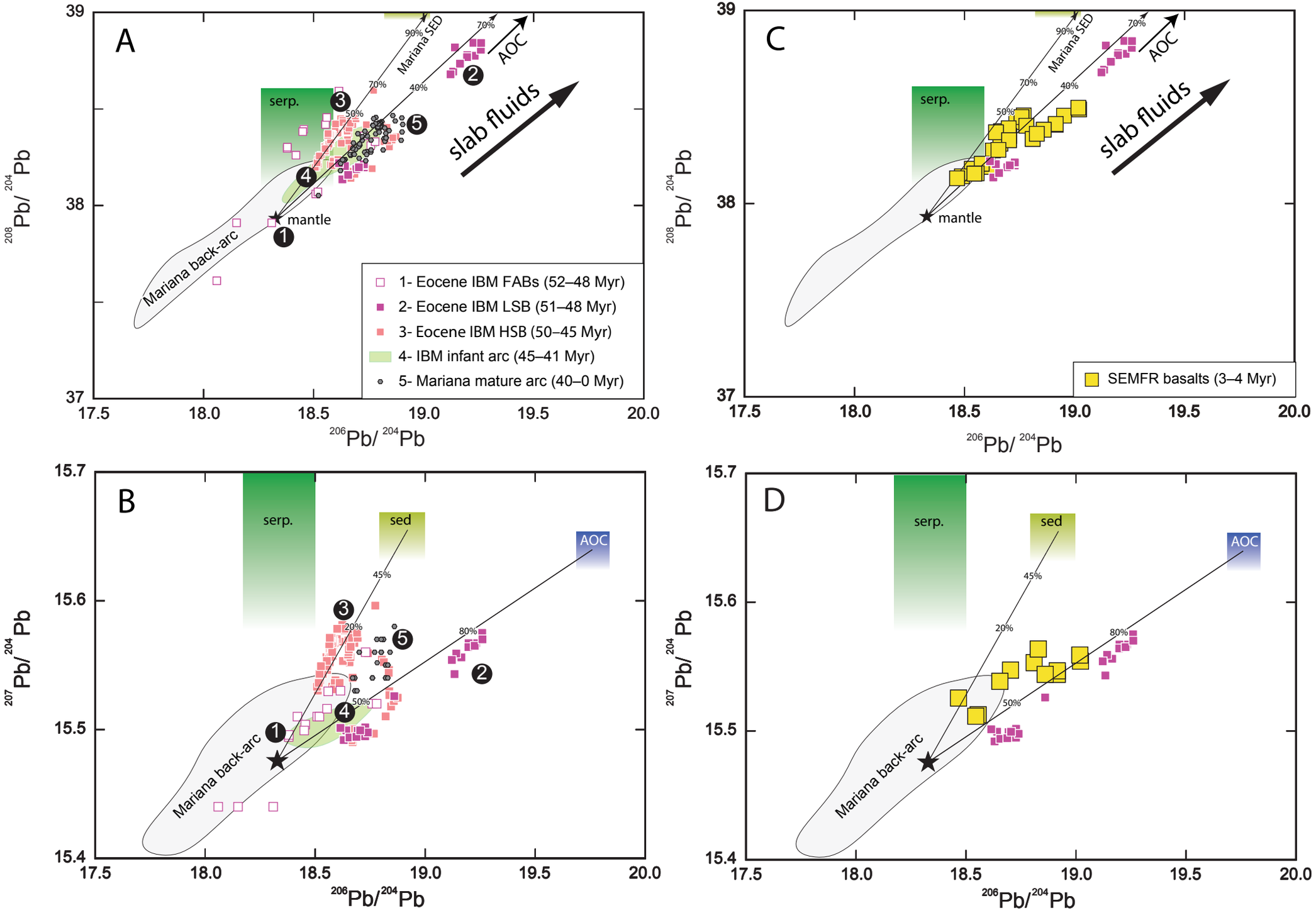
A
B
C
D
serp.
sed
AOC
mantle
slab fluids
Mariana back-arc
Mariana SED
90%
70%
50%
40%
45%
20%
80%
1
2
3
4
5
1- Eocene IBM FABs (52–48 Myr)
2- Eocene IBM LSB (51–48 Myr)
3- Eocene IBM HSB (50–45 Myr)
4- IBM infant arc (45–41 Myr)
5- Mariana mature arc (40–0 Myr)
SEMFR basalts (3–4 Myr)
$^{208}Pb/^{204}Pb$
$^{207}Pb/^{204}Pb$
$^{206}Pb/^{204}Pb$
39
38
37
15.7
15.6
15.5
15.4
17.5
18.0
18.5
19.0
19.5
20.0

A- Formation of the proto-arc crust in IBM

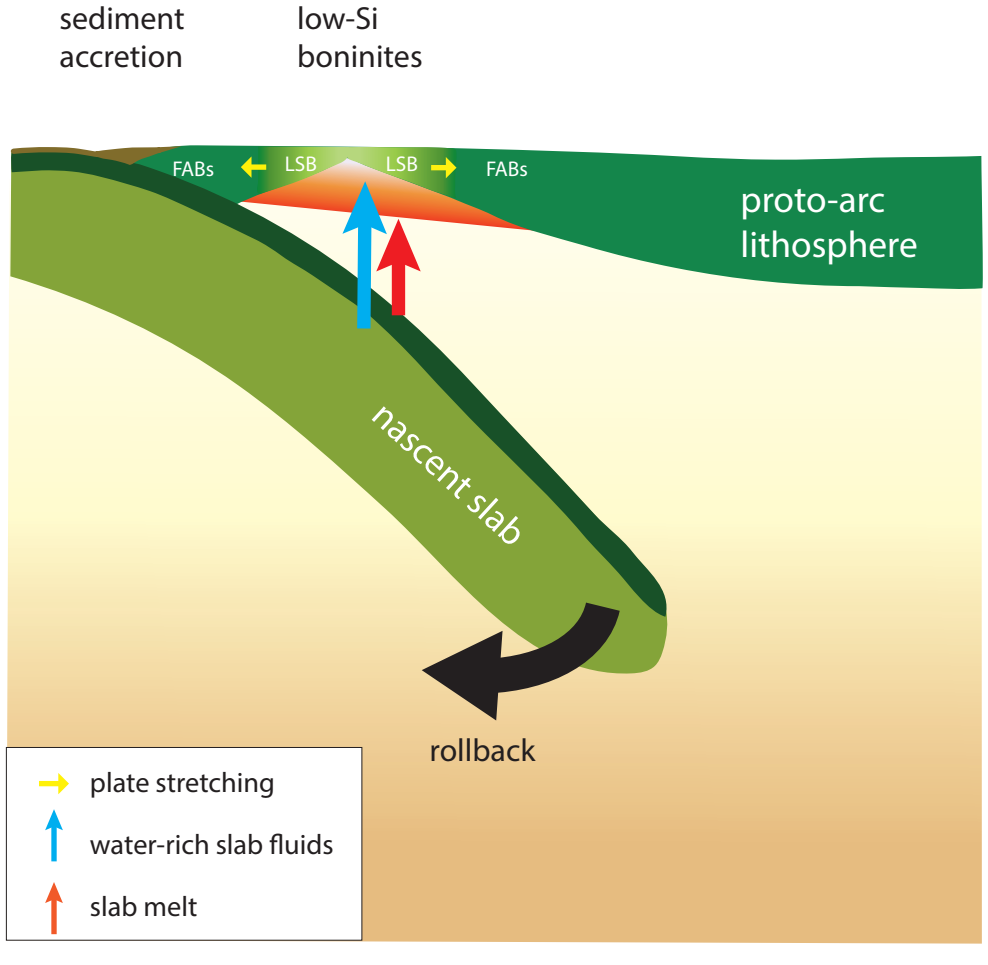

B- Arc infancy

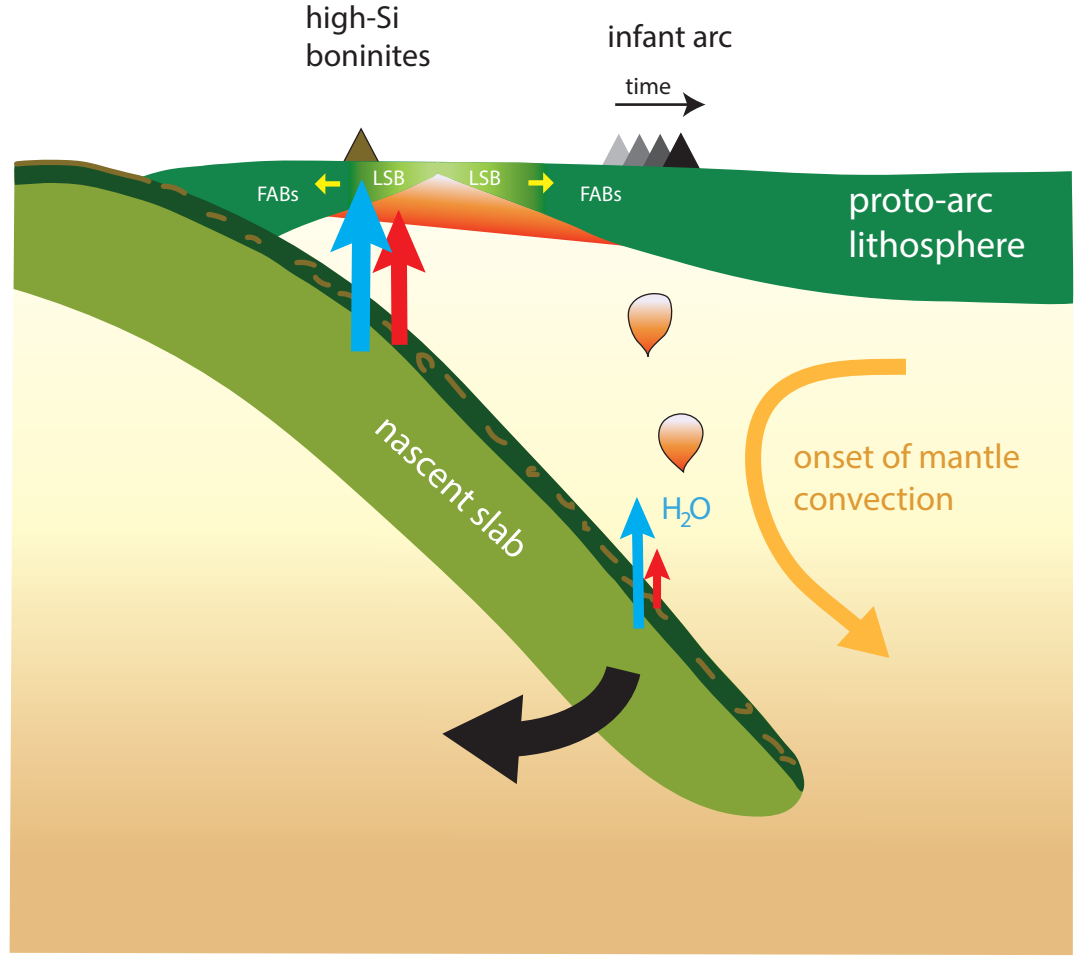

B- Mature intra-oceanic arc